Physics-driven digital twins to quantify the impact of pre- and postharvest variability on the end quality evolution of orange fruit

Daniel I. Onwude[1*], Flora Bahrami[1,2], Chandrima Shrivastava[1,2], Tarl Berry[4], Paul Cronje[4], Jade North[4], Nicola Kirsten[5], Seraina Schudel[1], Eleonora Crenna[3], Kanaha Shoji[1], Thijs Defraeye[1*]

[1] *Empa, Swiss Federal Laboratories for Materials Science and Technology, Laboratory for Biomimetic Membranes and Textiles, Lerchenfeldstrasse 5, CH-9014 St. Gallen, Switzerland*

[2] *University of Bern, ARTORG Center for Biomedical Engineering Research, Mittelstrasse 43, CH-3012 Bern, Switzerland*

[3] *Empa, Swiss Federal Laboratories for Material Science and Technology, Technology and Society Laboratory, Lerchenfeldstrasse 5, CH-9014 St. Gallen, Switzerland*

[4]*Citrus Research International, Department of Horticultural Science, University of Stellenbosch, Private Bag X1, Stellenbosch 7602, South Africa*

[5]*CITRII, Postharvest Research division, Lucern packhouse, Robertson, South Africa*

Currently, there are differences in the quality loss between individual fruit upon arrival at retail. These differences in fruit quality stem from pre-harvest biological variability between individual fruit at harvest and postharvest variations in hygrothermal conditions between refrigerated shipments. The impact of these pre-harvest biological and postharvest variability on the final quality of each fruit that reaches the consumers remains largely uncharted. Here, we address this gap by developing physics-based digital twins of orange fruit to unveil how pre-harvest and postharvest variability affect the final fruit quality upon arrival at retail. We use the Markov chain Monte Carlo method to generate a realistic 'virtual' population of 1000 individual orange fruits at harvest. We then quantify the impact of pre-harvest biological variability and variations in hygrothermal conditions between shipments on several orange quality metrics, including mass loss, fruit quality index (FQI), remaining shelf life (RSL), chilling injury severity (CI), total soluble solids (TSS), color, and Mediterranean fruit fly (MFF) mortality. We show that pre-harvest biological variability causes variations in mass loss of oranges at retail by up to 1.2%, FQI by up to 5% and RSL by more than 2 days. Our results demonstrate that postharvest variability between shipments causes high variations in mass loss of oranges at retail by up to 4%, FQI by more than 20%, RSL up to 3 days, and CI up to 5%. We also show that compared to pre-harvest biological variability, postharvest variability between shipments could increase the variations in RSL of oranges at retail by 75%, FQI by 50%, and mass loss by ~10%. This work helps improve our understanding of the variability in the end fruit quality upon arrival at retail.

[*] *Corresponding author: daniel.onwude@empa.ch (D.I Onwude) Empa, Swiss Federal Laboratories for Materials Science and Technology, Laboratory for Biomimetic Membranes and Textiles, Lerchenfeldstrasse 5, CH-9014 St. Gallen, Switzerland*

Nomenclature

Symbols

ρ_i	Density of material [kg·m^{-3}]
C_{pi}	Specific heat capacity of material [J·kg^{-1}·K^{-1}]
λ_i	Thermal conductivity of the material [W·m^{-1}·K^{-1}]
Q_{resp}	Volumetric heat of respiration [W·m^{-3}]
n	Unit vector normal to the surface
h_c	Convective heat transfer coefficient [W·m^{-2}·K^{-1}]
T_{air}	Delivery air temperature [K]
j_m	Moisture flux at the surface [kg·m^{-2}·s^{-1}]
H_{vap}	Latent heat of evaporation [J·kg^{-1}]
ϕ	Porosity in a pallet of orange fruits [%]
Q_{air}	Delivery air flow rate [m^3·h^{-1}]
$u_{superficial}$	Superficial airspeed [m·s^{-1}]
A_{cross}	Cross-sectional area of the bottom of the cargo space [m^2]
$u_{physical}$	Speed of the air confined in the porous medium [m·s^{-1}]
D_{fruit}	Diameter of the orange fruit [m]
r_{pulp}	Radius of pulp [mm]
$rind_{thick}$	Rind thickness [mm]
Nu	Nusselt number
Re	Reynolds number
ν_{air}	kinematic viscosity of air [m^2 s^{-1}]
Pr	Prandtl number for air
μ_{air}	Absolute viscosity of air [kg m^{-1} s^{-1}]
$\mu_{air,\ wall}$	Viscosity of air at the wall [kg m^{-1} s^{-1}]
T_{ini}	Initial air temperature [°C]
a_w	Water activity below the fruit surface [%]
$\delta_{wv,air}$	Diffusion coefficient of water vapor in the air [m^2 s^{-1}]
k_t	Convection mass transfer coefficient [ms^{-1}]
$P_{v,rind}$	Surface/rind vapor pressure [Pa]
$P_{v,air}$	Ambient vapor pressure [Pa]
k_{rind}	Moisture migration through the rind [s·m^{-1}]
k_{air}	Air film mass transfer coefficient [s·m^{-1}]
Sc	Schmidt number
P_{sat}	Saturated vapor pressure [Pa]
P_{atm}	Atmospheric pressure [Pa]
Y	Absolute humidity [kg/kg]
h	Enthalpy [kJ/kg]
T_{rind}	Surface/rind temperature [K]
T	Temperature [K]
C_{pair}	Specific heat capacity of air [J·kg^{-1}·K^{-1}]
RH_{air}	Relative humidity of the air [%]
A_s	Surface area of the fruit [m^2]
m_{ini}	Initial mass of the fruit [kg]
k_i	Rate constant [s^{-1}]
n_i	Order of the reaction
A_i	Quality attributes

$E_{a,i}$	Activation energy [J mol^{-1}]
R	Ideal gas constant [J mol^{-1} K^{-1}]
$F_{cumulative,T_{ref}}$	Cumulative process lethality
T_{core}	Core temperature [K]
T_{ref}	Reference temperature [K]
T_{db}	Dry bulb temperature of air [^{o}C]
t	Time (s)
D_{Tref}	Time required to obtain a log reduction of fruit fly (a specific temperature) [days]
N_0	MFF survivors at the start (t=0)
$N(t)$	MFF survivors at any time instant (t) of the process
Ω(t)	Damage integral as a function of time [-]
$k_{0,ci}$	Pre-exponential factor [s^{-1}]
$E_{a,ci}$	Activation energy for chilling injury [J·mol^{-1}]
$CI_{incidence}$	Incidence of chilling injury [%]
I	Respiration-driven quality indicator [%]
A_0	Initial fruit quality
$k_{0,quality}$	Quality rate constant [s^{-1}]
$E_{a,quality}$	Activation energy for fruit quality [J·mol^{-1}]
TSS	Total soluble solids [°Brix]
Col	Color [score 1-5]

Abbreviations

SHR	Sensible heat ratio
IQR	interquartile range
RSL	Remaining shelf life [days]
STDev	Standard deviation
MCMC	Markov chain Monte Carlo
CI	Chilling Injury [%]
FQI	Fruit quality index [%]
ML	Mass loss [%]
MFF	Mediterranean Fruit Fly
SC	Supply chain
DC	Distribution center

1 INTRODUCTION

Every year, about one-third of the world's fresh produce is lost within the food supply chain, from farm to consumer [1], [2]. Such a remarkable level of food loss amounts to an enormous loss in water, labor, and investment, and also contributes to 5 - 10% of global greenhouse gas emissions [3]–[5]. Still, it is not fully understood when or why food loss occurs within hundreds of fresh produce shipments in a supply chain, let alone the best way to reduce such loss. One reason is that each fruit has a unique pre-harvest biological properties with which it starts its postharvest journey, depending on its growing conditions and harvest time. These fruit properties result from biochemical and physiological processes, such as pigment synthesis and carbohydrate accumulation influenced by growing conditions [6], [7]. Due to varying growing conditions, the differences in the biological properties of individual fruits at harvest affects the quality of fresh produce in the subsequent stages of the postharvest supply chain, especially at the consumer [8]–[10].

The postharvest supply chain is often characterized by refrigerated storage and transport logistics during the entire journey of fresh produce [11]. These refrigerated shipments contain environmental air temperature and humidity sensors. Data from these sensors are often used as the first indicator to map the quality evolution in such shipments. For these, the low temperatures maintained decrease the rate of temperature-driven biochemical degradation reactions, thereby increasing the quality and remaining shelf life of fresh produce. However, every refrigerated shipment encounters a distinct hygrothermal journey. The reasons for this include variability in environmental air temperature and humidity, delays at ports, routing changes, or possibly cooling breakdowns [12]. Since the time-varying environmental air temperature and humidity profile is different for every shipment, each shipment has a peculiar food quality evolution. This variability is another reason why there are large variations between individual fruits upon arrival at the retailer, that is to say, some fruits will degrade sooner than others. Excessive decay could lead to the complete discard of the full shipment of fruits or require laborious sorting out of the spoiled products.

Research has been conducted on how biological variability of fresh produce at harvest [13]–[19] and postharvest variability between shipments [15], [20] affect the quality of fruits. Rarely, the impact of several pre-harvest biological properties of fruits at harvest and hygrothermal differences between shipments are accounted for. Additionally, in most cases, the targeted cold chain scenarios do not reflect the fluctuations in air temperature or the duration of actual transcontinental cold chains and their impact on storage life variability. To the best of our knowledge, information on why and when food loss occurs at the end of the fresh produce supply chain does not exist. To this end, the relevant question is what has the highest impact on the quality of fruits that a consumer receives. We need to know if (i) the variability in the initial quality at the onset of the cold chain, or (ii) the variability in environmental conditions the fruit experiences between different shipments has the most significant impact on the quality of fruits the consumer receives.

To answer these questions, this study aims to quantify the impact of pre-harvest biological variability of fresh fruits at harvest and postharvest variability due to hygrothermal differences between shipments on the end quality evolution of orange fruit. We used a hybrid Markov Chain Monte Carlo (MCMC) method and physics-based mechanistic digital twin to unveil the impact of the pre-harvest biological variability of Valencia oranges on fruit quality evolution in a single shipment. A mechanistic digital twin of fruit is a 'virtual' model linked to real-world processes via sensor data, containing all essential product characteristics and simulating relevant hygrothermal and metabolic processes of the fruit (Figure 1)[21]–[23]. MCMC was used to generate a realistic 'virtual' population of orange fruits with different physical and geometrical properties. With this approach, digital twins of 1000 'Valencia' oranges (16 cartons-1/5 pallets of oranges) were developed to simulate ongoing quality evolution in a single shipment. These simulations indicate how much the biological variability in the shipment affects the end quality. We also quantified the impact of postharvest variability due to hygrothermal differences between shipments on the quality evolution of oranges. These simulations indicate how much the specific shipment of fruits affects the end quality. Finally, we compared the impact of pre-and postharvest variability on the quality of oranges at the retail to identify the value chain with the most impact.

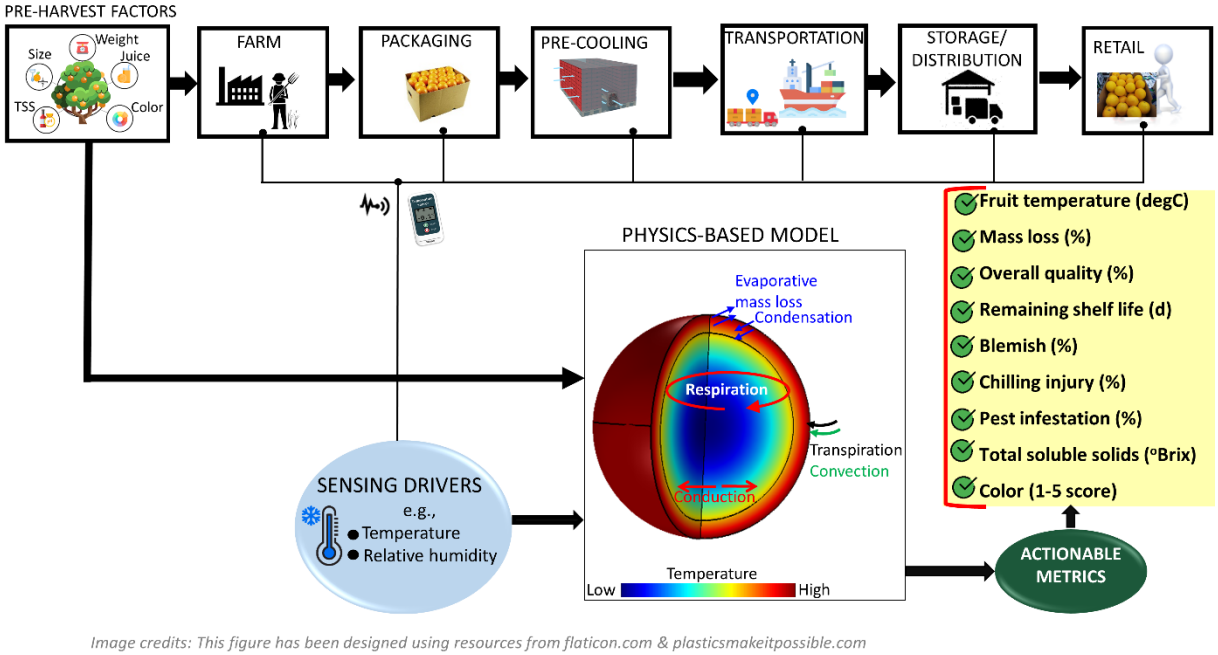

Image credits: This figure has been designed using resources from flaticon.com & plasticsmakeitpossible.com

Figure 1. A digital twin of a typical citrus supply chain from the farm until the consumer at retail level.

2 MATERIALS AND METHODS

2.1 Data collection

2.1.1 Biological properties of fruit at harvest

The study was carried out for 'Valencia' orange over the 2019 season in the Citrusdal production area, Western Cape, South Africa. Except where stated otherwise, all fruit were harvested at commercial harvesting maturity as determined by producers. Five fruits per tree were harvested from two trees in five different orchards. A total of fifty oranges were sampled and data were collected for different physicochemical properties.

The external fruit properties such as fruit weight (g) and rind weight (g) were determined at harvest using an electronic scale (ADW, UWE Scales and Calibrations, Cape Town, South Africa). The fruit size (mm) and rind thickness (mm) were measured using a caliper (CD-6" C, Mitutoyo Corp, Tokyo, Japan) after the seven-day shelf-life period. The rind color for each fruit replicate was obtained using the standard CRI colour plate (CRI, 2004) for orange, where a visual color score is assigned to each fruit.

The internal properties of the fruit were assessed by cutting along the longitudinal plane of the fruit for juice extraction using a citrus juicer (8-SA10, Sunkist®, Chicago, USA). The total sugar content of the fruit pulp (measured as °Brix and expressed as % TSS in the pulp) was determined using a digital refractometer (PR-32 Palette, ATAGO CO, Tokyo, Japan).

2.1.2 Measurement of air temperature in actual cold chain

The air temperature on the cold chain of oranges was monitored and data from TempTale®4 (TT4) GEO Eagle Extended (SENSITECH, Beverly, MA, USA) sensors with an accuracy of ±0.5 °C were acquired. Data acquired are for 43 shipments from packhouse in Durban, South Africa, to a distribution center (DC) in Western Europe spanning an entire season (August 2018 to September 2019). This data provides realistic temperature data for overseas cold chain. The air temperature sensors were positioned in the second last row of pallets from the door on the left-hand side of the container at half the height of the pallet (see supplementary material for details). The targeted delivery air temperature for these shipments was between -1 °C to 0 °C. Note that a sample size of 43 shipments of 'Valencia' oranges was found sufficient for this study using a modified Cochran's formula with 95% confidence level and ±5% precision [20]. We also showed this by examining the minimum required sample size that stabilizes the average air temperature value. Specifically, for this study, the minimum amount of dataset with 95% confidence interval for the average air temperature values (°C) is 5 and above. Details of the estimation procedure are provided in the supplementary material.

To further extend the monitored supply chain from the DC to retail storage, three days retail sales conditions were assumed and added to the sensor data, with a daily time interval of 3600 s for each shipment. This was simulated stochastically based

on the average air temperature (°C) at several retail locations in Rotterdam, Netherlands, collected via NASA POWER (August 2018 to September 2019). The average air temperature for the locations was for specific retail storage days and times of the month based on each shipment time stamp at DC. In addition, the standard deviation of the measured cold chain air temperature (°C) was also used for the stochastic simulation.

2.2 Markov chain Monte Carlo sampling

We developed the MCMC algorithm using Gibbs sampling with package NMixMCMC in Rstudio software (version 1.4.1106)[24]. We then generated a population of 1000 realistic 'virtual' orange fruits, which are fed into a physics-based digital twin as input data for the stochastic simulation (see sections 2.3 and 2.4). To do this, we considered a prior probability distribution of 'Valencia' orange (i.e., the mean and standard deviation of different pre-harvest biological properties from literature)[25]–[29]. We also considered a field sample dataset of 50 'Valencia' oranges of different pre-harvest biological properties with 10 oranges each from five different orange orchards in Citrusdal, South Africa. The pre-harvest biological properties of fruit at harvest include fruit size (mm), fruit weight (g), TSS (°Brix), fruit color (color chart 1-5 scale), rind thickness (mm), rind weight (g), initial quality (%), fruit density (kg m^{-3}), and rind density (kg m^{-3}). More details about the MCMC method and steps are given in the supplementary material.

2.3 Digital twin configuration

A physics-based mechanistic model based on the finite element method was developed to simulate the quality evolution of 1000 'Valencia' oranges (*Citrus sinensis* (L.) Osbeck) in a refrigerated container. A single fruit was modeled as a two-dimensional axisymmetric geometry of a sphere (Figure 2). The domain was divided into two sections of the fruit – the rind (base case thickness ($rind_{thick}$) = 5.9 mm) and the fruit pulp (base case radius (r_{pulp}) = 30.7 mm). The configuration was simplified, and the fruit-fruit interaction was ignored. This means that the limited thermal interaction with other fruit is ignored, due to the few contact points between fruits, and the fact that surrounding fruit is at a similar temperature. The model was calibrated with the same geometrical and material properties as the real fruit and linked to a sensor and virtual orange data, thus forming digital twins of oranges in a supply chain.

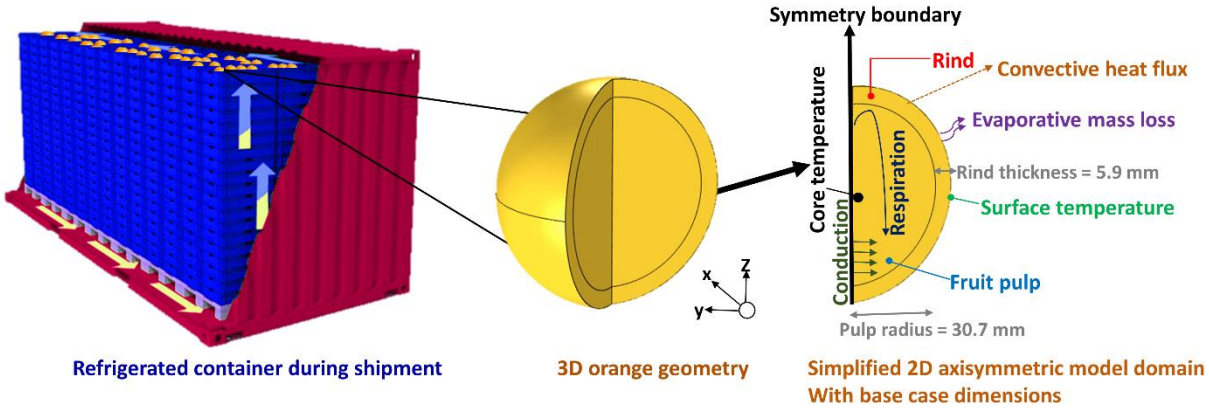

Figure 2. Geometry and boundary conditions of an orange in a refrigerated shipping container (figure not to scale).

2.4 Mechanistic multiphysics model

A continuum mechanistic model was developed to calculate heat transfer inside the orange fruit and its convective exchange with the environment throughout the supply chain from farm to retail. In addition, physics-based models for predicting mass loss, thermally-driven fruit quality index, pest mortality, and chilling injury were also coupled with the thermal model for heat transfer.

2.4.1 Thermal model

The energy conservation equation was solved in the fruit, with temperature (T, K) as the time-dependent variable (Equation. 1).

$$\rho_i C_{p,i} \frac{\partial T}{\partial t} + \nabla \cdot (-\lambda_i \nabla \mathrm{T}) = Q_{resp,i} \qquad (1)$$

where ρ_i is the density (kg·m^{-3}), $C_{p,i}$ is the specific heat capacity (J·kg^{-1}·K^{-1}), λ_i is the thermal conductivity of the material (W·m^{-1}·K^{-1}), with the subscript i corresponding to the rind and fruit pulp. Q_{resp} (W·m^{-3}) is the volumetric heat of respiration, which is the product of heat of respiration (W kg^{-1}), multiplied by the pulp density (kg m^{-3}). The heat of respiration was estimated from a correlation between the carbon dioxide production rate of orange and the temperature [30] (see supplementary material for details). Thermal equilibrium between all components and phases was assumed in this model. The material properties are given in Table 1.

The convective boundary condition for heat transfer based on flux continuity is presented in Equation. 2. The conductive flux within the fruit is balanced by the heat flux due to convection and evaporation at the surface.

$$\mathbf{n}.(\lambda \nabla T) = h_c(T_{air} - T) - j_m.H_{vap} \quad (2)$$

where **n** is the unit vector normal to the surface, h_c is the convective heat transfer coefficient (W·m^{-2}·K^{-1}), T_{air} is the delivery air temperature (K). Here j_m is the moisture flux at the surface (kg·m^{-2}·s^{-1}) derived from the moisture transport model (section 2.4.2) and H_{vap} is the latent heat of evaporation (H_{vap} = -2364.2T+3147175.2 J·kg^{-1}) [31].

The radiation exchange between different fruit inside the ventilated boxes was considered limited compared with convective heat transfer. This is because of the small temperature difference between adjacent fruit during cooling in actual cold chains. Thus, radiation exchange was not modeled.

Since the airflow field around the fruit was not explicitly modeled, its influence on the hygrothermal behavior of the fruit was accounted for using the convective heat and mass transfer coefficients (h_c, k_{air}). A representative airspeed in the porous stack of products, namely a pallet of orange fruit, was estimated based on the airflow rate inside a refrigerated container [32]. Equation 3 was employed to estimate the physical airspeed in the porous medium [33](see supplementary material for details). This physical airspeed is the actual speed around the orange fruit, which was 0.11 m·s^{-1} in the present study.

$$u_{\text{physical}} = \frac{u_{\text{superficial}}}{\phi} = \frac{Q_{air}}{A_{cross} \times \phi} \quad (3)$$

where u_{physical}, (m·s^{-1}) is the actual airspeed around the orange fruit, $u_{\text{superficial}}$, (m·s^{-1}) is the superficial airspeed, ϕ (%) is the porosity in a pallet of orange, A_{cross}, (m^2) is the cross-sectional area of the cargo bottom, and Q_{air} (m^3·h^{-1}) is the delivery air flow rate.

In this study, spatially-constant heat transfer coefficient (h_c, W·m^{-2}·K^{-1}) around the fruit in a container was assumed over the entire fruit surface, as a simplified representation even though h_c could spatially be distributed over the fruit surface [34]. The dependency of heat transfer coefficient (h_c, W·m^{-2}·K^{-1}) on airspeed is accounted for using the Nusselt number (Nu) correlation for flow around a single sphere presented in Equation 4 [35].

$$Nu = \frac{h_c D_{fruit}}{\lambda_{fruit}} = 2 + (0.4Re^{0.5} + 0.06Re^{0.667})Pr^{0.4}\left(\frac{\mu_{air}}{\mu_{air,wall}}\right)^{0.25} \quad (4)$$

where D_{fruit}[=2(r$_{\text{pulp}}$+rind$_{\text{thick}}$)] is the diameter of the orange fruit (m), Re (= D_{fruit}·u_{physical}·ν_{air}^{-1}) is the dimensionless Reynolds number as a function of the air speed, Pr is the Prandtl number for air, and ν_{air} is the kinematic viscosity of air. μ_{air} and $\mu_{\text{air, wall}}$ correspond respectively to the absolute viscosity of air and the viscosity of air at the wall, which were considered as equal in this study. The base case h_c value for this study is 4.6 (W·m^{-2}·K^{-1}).

Table 1. Base case input and thermal parameters of orange fruit

Properties	T_{ini} [°C]	$u_{physical}$ [m s^{-1}]	h_c [W m^{-2} K^{-1}]	k_{air} (10^{-3}) [ms^{-1}]	k_{rind} (10^{-9}) [sm^{-1}]	a_w [%]	ρ [kg m^{-3}]	λ [W m^{-1} K^{-1}]	C_p [KJ kg^{-1} K^{-1}]	ν_{air} (10^{-5}) [m^2 s^{-1}]	Pr	Re	Nu	Sc	μ_{air} (10^{-5}) [kg m^{-1} s^{-1}]	$\delta_{wv,air}$ (10^{-5}) [m^2 s^{-1}]
Pulp		-	-	-	-	100	1004.30	0.58	3.66	-	-				-	-
Rind	-	-	-	-	1.72	-	800.00	0.40	3.30	-	-				-	-
Air	20	0.11	4.58	4.65	-	-	1.25	0.02	1.01	1.46	0.74	540.11	13.87	0.67	1.79	2.19

2.4.2 Mass loss model

Mass loss, also called moisture loss, is a crucial metric in the cold citrus chains because it directly influences market value. As citrus is a product sold by weight, a loss in saleable weight implies a direct loss in profits. The mass flux (j_m), or moisture flux at the surface of the fruit (kg·m^{-2}·s^{-1}), was calculated as the product of the convective mass transfer coefficient (k_t), and the difference between surface vapor pressure ($P_{\text{v,rind}}$, Pa) and ambient vapor pressure ($P_{\text{v,air}}$, Pa) (Equation 5). These vapor pressures were estimated based on the surface temperature, ambient temperature, and ambient relative humidity (Equations 8-10). The mass transfer coefficient, k_t was determined from the contribution of the resistance due to moisture migration through the rind (k_{rind}, s·m^{-1}) and the resistance to mass transfer due to the air boundary layer (k_{air} s·m^{-1}) (Equation 6)[30], [36].

$$j_m = k_t.(P_{v,rind} - P_{v,air}) \quad (5)$$

$$k_t = \left(\frac{1}{k_{air}} + \frac{1}{k_{rind}}\right)^{-1} \quad (6)$$

The air film mass transfer coefficient (k_{air}) was estimated based on the airspeed (u_{air}, m·s^{-1}) using the Sherwood correlation for a sphere, as presented in Equation 7[30], [37].

$$Sh = \frac{k_{air} D_{fruit}}{\delta_{wv,air}} = 2 + (0.552\,\mathrm{Re}^{0.53} \cdot Sc^{0.33}) \quad (7)$$

where D_{fruit} is the diameter of the citrus fruit (m), Re (=$D_{fruit} \cdot u_{air} \cdot \nu_{air}^{-1}$) is the dimensionless Reynolds number as a function of the airspeed. Here, ν_{air} corresponds to the kinematic viscosity of air [m^2 s^{-1}], Sc (=$\nu_{air} \cdot \delta_{wv,air}^{-1}$) is the Schmidt number, $\delta_{wv,air}$ is the diffusion coefficient of water vapor in the air [m^2 s^{-1}]. The base case Sherwood number *(Sh)* for this study is 15.56 (see supplementary material for more explanation).

The vapor pressure was dynamically linked with temperature using the Antoine equation [30], expressed in Equation 8:

$$P_{sat} = \exp\left(23.4795 - \frac{3990.5}{T - 39.317}\right) \quad (8)$$

Specifically, the vapor pressure just below the rind ($P_{v,rind}$) was computed using Equation 9.

$$P_{v,rind} = P_{sat}(T_{rind})\ x\ a_w \quad (9)$$

where a_w is the water activity below the fruit surface [-] (Table 1).

While the vapor pressure of the air around the fruit ($P_{v,air}$, Pa) was estimated using the relative humidity of the air (RH_{air}, %), as shown in Equation 10.

$$P_{v,air} = RH_{air}\ x\ P_{sat}(T_{air}) \quad (10)$$

The relative humidity of the air within the refrigerated container (RH_{air}, %) was estimated using the principles of psychrometry, by assuming a constant sensible heat ratio (*SHR*) within the refrigerated container. Details of the calculation steps are included in the supplementary material.

Additionally, the transpiration-driven mass loss (*ML*, %) was computed using Equation 11.

$$ML = \frac{\Delta j_m \cdot A_s}{m_{ini}}\ x\ 100 \quad (11)$$

where A_s is the surface area of the fruit (m^2) computed from the geometry and m_{ini} is the initial mass of the orange (kg) which was measured as 0.21kg. Note that the threshold for citrus moisture loss during shipment is between 7 – 10% [38].

2.4.3 Thermally-driven model for fruit quality attributes

The quality of the fruit, which often determines consumer acceptability, is affected by temperature conditions during the cold chain from farm to retail. Most of the temperature-induced underlying biochemical reactions responsible for quality changes of oranges can be adequately modeled. The evolution of multiple quality attributes such as total soluble solids (TSS [°Brix]), color (Col [scale 1-5]) and fruit quality index ([%]) of the orange fruit can thereby be predicted.

For this purpose, kinetic rate law models were implemented in order to quantify the change with shipment time for each of the above-mentioned specific quality attributes A_i [39], [40], as in Equation 12:

$$\frac{-dA_i}{dt} = k_i A_i^{n_i} \quad (12)$$

where the subscript i indicates the specific attribute, k_i is the corresponding rate constant [s^{-1}], and n_i is the order of the reaction, which depends on the attribute's decay kinetics. The order of the reaction was chosen based on the best fit of the model with the data or the inherent order of the decay reaction (e.g., TSS is a first-order reaction, Table 2). However, little differences were often present between first- and zero-order approximations.

In Equation 12, for a constant value of k, i.e. at a constant temperature, the quality attribute decreases linearly over time (for zero-order reactions, where indeed the magnitude of the slope equals to k, Equation 13), or shows an exponential decrease (for first-order reactions, Equation14):

$$A_i(t) = A_{0,i} - k_i(T)t \quad (13)$$

$$A_i(t) = A_{0,i}e^{-k_i(T)t} + C_i \quad (14)$$

where $A_{0,i}$ is the quality attribute at the start of the cooling process (t = 0 s) for a specific attribute i and C_i is an integration constant.

However, in reality, the rate constant k_i is not constant, and so Equation (12) needs to be explicitly solved over time. The temperature dependency of the quality attribute was therefore incorporated into the rate constant through an Arrhenius relationship [39] as in Equation 15:

$$k_i(T) = k_{0,i}e^{\frac{-E_{a,i}}{RT}} \quad (15)$$

where $k_{0,i}$ is a constant [s^{-1}], $E_{a,i}$ is the activation energy [J mol^{-1}], R is the ideal gas constant (8.314 J mol^{-1} K^{-1}), and T is the absolute temperature [K]. For fruit quality index, color and total soluble solids of degree fruits, the constants $k_{0,i}$ and $E_{a,i}$, were calibrated from quality attribute data as a function of time at (at least) two different temperatures. More details are available in the supplementary material.

The fruit quality index (*I, %*), which is linked to the remaining shelf life at the retail, serves as a general indicator of the marketability of the fruit. The quality threshold value of 10% was assumed as a point where the product has not lost its quality completely, but first visual damage occurs, below which the product is not acceptable anymore to the consumer. This quality metric was modeled using a first-order kinetic model, which quantifies the respiration-driven, temperature-dependent change in overall quality from the point of harvest until the point where the fruit is considered to be lost [41]. Details of the model calibration are presented in the supplementary material.

The remaining days of shelf life (RSL) for a shipment were predicted based on the same kinetic rate model, by storing the fruit in-silico at retail air condition of 20 °C. Here, typical dynamic conditions encountered during retail were also considered. *RSL* was computed until the remaining quality of the respiration-driven quality indicator (*I*) attained the threshold of acceptable quality (≥20%). The base case quality parameter values used for the physics-based simulation of orange fruit are presented in Table 2.

Table 2. Base case quality parameters of orange fruit

Kinetic-rate-law model parameters for the quality attribute of orange fruit										
Parameter		Symbol	A_0	C	n	E_a [J.mol^{-1}]	k_0 [s^{-1}]	Q_{10}	$k_{0,quality}$ [s^{-1}]	$E_{a,quality}$ [J.mol^{-1}]
Fruit index	quality	*I* (%)	80.00 %	0	1	-	-	2.00	148	45229
Color		Col (score 1-5)	1.80	0	0	44585	17	2.00	-	-
Total solids	soluble	TSS (°Brix)	12.04 °Brix	0	1	49524	-1	2.00	-	-

2.4.4 Lethality model for pest mortality

We modeled the efficacy of the cold disinfestation treatment against Mediterranean fruit fly (MFF) based on a lethality model [42]. This was done based on knowledge of the time-temperature history of the fruit at its most critical location, with the highest temperature during cooling. For citrus fruit, the most critical location corresponds to the core of the fruit. This model, described in the supplementary material, was calibrated based on the death kinetics of Mediterranean fruit fly [43].

2.4.5 Thermal damage model for chilling injury

Chilling injury is a physiological disorder caused by suboptimal low storage temperature beyond a threshold duration that alters the tissues in the rind, leading to symptoms such as peel pitting or discolorations that render the fruit unmarketable [44], [45]. The incidence of chilling injury on the surface of the fruit was computed similarly to the thermal damage model for the human

skin during skin burn [46]. The model, described in the supplementary material, quantifies thermal damage as a dimensionless damage integral (Ω) based on the combined effect of rind temperature ($T_{rind,}$) (K) and exposure time (t).

2.5 Numerical simulation

The physics-based digital twin was implemented in COMSOL Multiphysics (version 5.6), which is a finite element-based commercial software. The transient conductive heat transfer and thermal damage model in the fruit during convective air cooling was solved using the 'Bioheat Transfer' physics. Ordinary Differential Equations' and 'Differential Algebraic Equations' interfaces were used to solve for moisture transport, total soluble solids, color, fruit quality index, and mortality of fruit fly. Quadratic Lagrange elements were used together with a fully-coupled direct solver, relying on the MUMPS (MUltifrontal Massively Parallel sparse direct Solver) solver scheme. The solver tolerance was set to 10^{-5} based on sensitivity analysis. Adaptive time-stepping based on the Backward Differentiation Formula (BDF) was used for the simulation, with the maximum step set to automatic to maintain the desired relative tolerance. A grid sensitivity analysis was conducted to ensure that the results were grid-independent (see supplementary material for details). The grid consisted of triangular and quadrilateral finite elements, with a total element size of 6504. To stochastically simulate the quality evolution of 1000 'Valencia' oranges via the digital twins, we performed a parametric sweep over the wide range of pre-harvest biological properties of fruit generated from MCMC. The parametric sweep feature in COMSOL Multiphysics® runs calculations for several parameter cases in a single instance.

2.6 Statistical data and sensitivity analysis

The actionable quality metrics from the digital twins were analyzed and presented as median (centre line), 75^{th} upper and 25^{th} lower quartiles (box limits) and 1.5 × the interquartile range (IQR, whiskers) with a 0.95 confidence level. We also used Levene's test at $p \leq 0.05$ significant level and 95% confidence interval to assess the equality of variances at farm level, port in South Africa (SA), port in Europe (EU), and retail storage within a single shipment.

We also presented the combined pre-harvest biological and postharvest variability assessment based on mean values of the different quality metrics at retail. A fitted probability distribution function and rug plot were applied to visually determine the statistical differences in quality evolution due to pre and postharvest variability at the end of the supply chain. Additionally, a two-sample t-test, assuming equal variances at $p \leq 0.05$ significant level, was used to compare the mean significant difference of the quality evolutions.

Sensitivity analysis was carried out to assess the impact of each pre-harvest biological property on fruit quality variability at the end of the cold chain (see supplementary material for details). The descriptive test, probability distribution function and sensitivity analysis were all conducted using ORIGIN 2020b (Government) (OriginLab, Northampton, Massachusetts, USA) and Microsoft Excel (2016).

3 RESULTS and DISCUSSION

3.1 Markov chain Monte Carlo (MCMC) analysis

To assess the variability of the oranges due to pre-harvest conditions at harvest, we first employed MCMC sampling method. MCMC used measured data to generate a statistically-representative set of fruit properties for individual fruits. With MCMC, we generated a realistic virtual population of orange fruit used for stochastic simulations via digital twins.

Figure 3 shows the correlation matrix between the different parameters of the sample data and also the generated virtual population. The point estimates, range, mean and standard deviation of the posterior distribution of the variance components were calculated from the MCMC samples. By comparing the correlation coefficient between parameters of sample data and the generated virtual oranges, MCMC successfully captures the realistic relationship between the different sample data parameters (so the properties as fruit size (mm), fruit weight (g), TSS (°Brix), fruit color (color chart 1-5 scale), rind thickness (mm) and rind weight (g)) and the corresponding parameters of the generated virtual oranges.

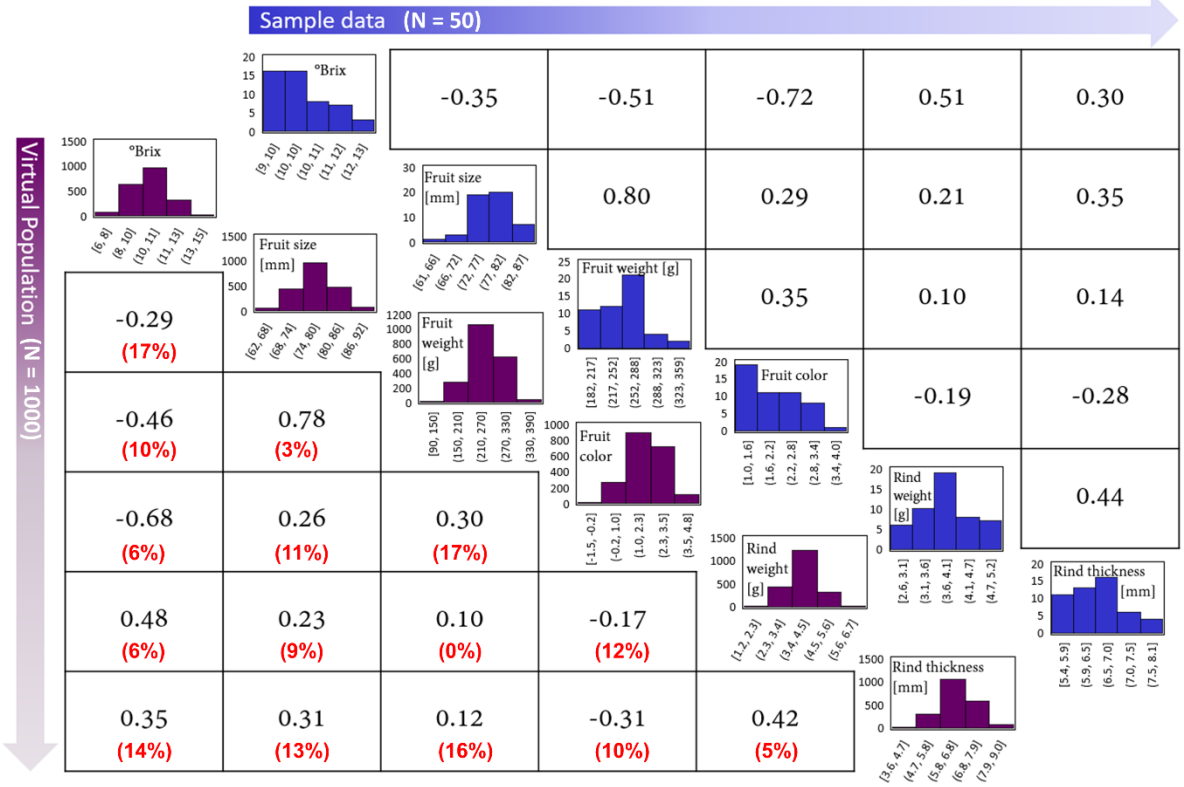

Figure 3. Correlation matrix between the parameters of pre-harvest sample data and the generated 'virtual' population showing the Pearson correlation and histogram. The percentage differences in the correlation coefficients between the sampled data and the virtual population are shown with the red-colored text.

3.2 Impact of pre-harvest biological variability on fruit quality evolution

We evaluate the impact of pre-harvest biological variability on fruit quality evolution. We therefore simulate 1000 orange fruits that are transported in a single shipment (i.e., -1°C targeted delivery cold air temperature and shipment length of 30 days). For a real shipment of citrus fruit in a refrigerated container, typically about 100'000 orange fruit are shipped in 20 pallets. Although we cover only 1% of this shipment, this sample size is already much larger than what is experimentally monitored during quality control and a statistically relevant sample size of the shipment. We quantified mass loss (%), fruit quality index (%), remaining shelf life (RSL) (days), chilling injury severity (%), MFF mortality (%), total soluble solids (TSS) (°Brix) and color (1-5 scale). Figure 4 shows box plots of the different quality evolution at different supply chain stages from South Africa (SA) to retail shops in Europe (EU) using the digital twin.

Figure 4A shows the variability in fruit mass loss from farm to retail due to pre-harvest biological variability. The mass loss increased across the postharvest supply chain and the variability between individual fruit increase slightly (standard deviation (STDev) up to 1% and relative STDev from 21% to 19%) as the shipment progresses further throughout the chain. Indeed, the pre-harvest biological variability of oranges results in a variation in fruit transpiration, which is directly correlated with mass loss [47], [48]. The largest mass loss occurs at retail (2% of initial fruit weight). The high amount of mass loss at retail is due to higher storage temperature, decreased humidity, and increased respiration heat production, as this is temperature dependent. Similar findings on increased respiration rates of fruits at higher temperatures have been reported [14], [49]. The impact of pre-harvest biological variability of orange fruits on mass loss is largest at retail. Due to inherent biological variability in fruit properties after harvest, the mass loss of a shipment shows a variability up to 1.2% between individual fruit. This is substantial given that the average mass loss of the entire shipment is 3.4% upon arrival at the retailer.

Figure 4B shows the impact of pre-harvest biological variability on the temperature-driven fruit quality index evolution of orange fruit. The fruit quality index and variability of the fruit decrease across the postharvest supply chain, with STDev ranging from 9% (farm level) to 4% (at retail). This means that the impact of pre-harvest biological variability on the fruit quality index of oranges decreases across the postharvest supply chain. The impact of pre-harvest variability of oranges is lowest at retail storage compared to the other supply chain stages. However, this impact is still high, with a fruit quality variability between individual fruits of the same shipment at retail of up to ~5%. This means that ~20% of the entire shipment upon arrival at retail contains fruits of different fruit quality, as the average fruit quality index is about 30%. This implication can be further seen in the remaining shelf life days between individual fruits at retail.

Using the quality upon arrival at the retailer, we quantified the remaining shelf life of each of the 1000 fruits in the shipment after arrival at the retailer. The average remaining shelf life of the shipment was 6 days, and the standard deviation was 1.4 days. The min and max values were 1.2 and 9.4 days, respectively. As such, variability in the remaining shelf life of several days was found between individual fruit.

Next, we assessed the influence of pre-harvest biological variability on the chilling injury severity of oranges within a shipment (Figure 4C). The chilling injury of oranges increased from 0% to 11.5% across the postharvest supply chain. Very high chilling injury occurred at the end of refrigerated shipment and during storage at retail, with values above the severe chilling injury threshold. A very low variation (<0.5%) in chilling injury was observed for the entire supply chain. This low variability is due to the minimal impact of fruit density and size (see sensitivity analysis in supplementary material). This implies that the pre-harvest biological variability does not have much impact on the chilling injury of oranges during shipment. Rather, the chilling injury was mainly driven by cold chain practices (e.g., low air temperature) (see section 3.3). Nonetheless, there is a significant difference between the variability at the beginning of the postharvest journey (0%) and the end of the retail storage (0.3%) ($p \leq 0.05$). Indeed, fruit sensitivity to low temperatures is also influenced by a variety of other pre-harvest biological factors such as biological age, harvesting time, production area, production season, pre-harvest temperature and humidity, and other cultural practices [9], [50]–[52]. All these pre-harvest factors were not considered in this study due to insufficient field data. Therefore, it was not possible to assess their actual impact on chilling injury.

The impact of pre-harvest biological variability on MFF mortality of oranges for a single shipment is presented in Figure 4D. In accordance with protocols dictated by citrus import regulations, maintaining a low delivery air temperature is essential to keep the fruit core temperature at or below 2 °C for 16.7 days or at 3 °C for 18 days. Thereby, at least 99.9968% Mediterranean fruit fly (MFF) mortality can be achieved [53]–[55]. In this study, the average MFF mortality increased from 0% to 100% across the postharvest supply chain, whereas the variability is less than 0.1%. This implies that the pre-harvest biological variability does not impact MFF mortality at the end of the supply chain. That is, the entire shipment upon arrival at the retailer is devoid of pest infestation. This also means that there are not many differences in core temperature between fruits of different sizes, once they are properly cooled down.

We also show the impact of pre-harvest variability on total soluble solids (TSS) (Figure 4E) and color (Figure 4F) evolution of oranges during shipment. There was no significant change in the TSS (Figure 4E) and color (Figure 4F) across the postharvest supply chain. This shows that the pre-harvest biological variability has an equal impact on TSS and color of degreened oranges across the entire supply chain. This is expected because 'Valencia' orange is a non-climacteric fruit and, as such, does not increase in TSS, or show a change in color at low (>4°C) shipping temperatures. Since TSS and color do not change for degreened citrus fruit after harvest, the variability between the different fruit after harvest will be the one that quality control experts upon arrival at the retailer will observe.

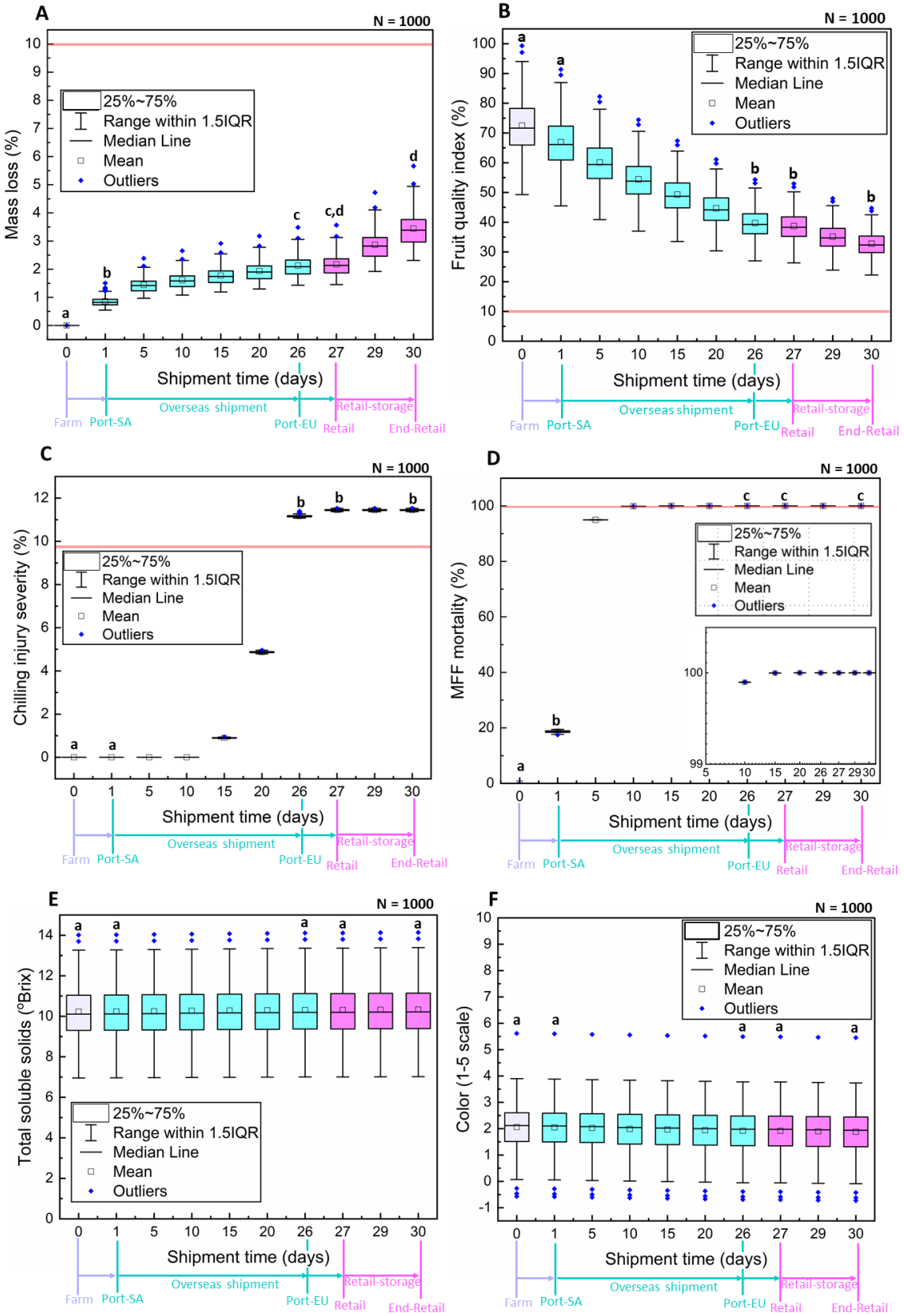

Figure 4. Propagation of pre-harvest parameter variability at different major stages along the cold chain of a single shipment (-1 °C targeted delivery cold air temperature and shipment length of 30 days) from farm in South Africa (SA) to retail shops in Europe (EU) for different quality metrics via digital twin; [A] mass loss (%), [B] fruit quality index

(%), [C] chilling injury severity (%), [D] Mediterranean fruit fly (MFF) mortality (%), [E] total soluble solids (°Brix), [F] color (1-5 scale). The fruit quality of 80% was assumed when leaving the packhouse calibrated based on measured quality data. The boxplots within represent the median (centre line), 75^{th} upper and 25^{th} lower quartiles (box limits) and 1.5× the interquartile range (whiskers) (IQR). Letter N at the top of the plot indicates the number of samples. Significant differences between different stages along the supply chain, namely, farm, port-SA, port-EU, arrival at retail and end of retail storage, were determined using the Levene's test of equal variances and are indicated with letters from a to d for statistical significantly different groups at $p \leq 0.05$. The red-colored horizontal line in the plots signifies the threshold value for the different quality metrics.

3.3 Impact of postharvest variability on fruit quality evolution

Here, we quantify the impact of postharvest variability due to hygrothermal differences between shipments. Therefore, we simulated a single fruit going through 43 different shipments. We quantified mass loss, fruit quality index (FQI), remaining shelf life (RSL) days, chilling injury and Mediterranean fruit fly (MFF) mortality of oranges at the end of the supply chain via digital twin. The total soluble solids (TSS) and fruit color were not considered as they remain constant through the supply chain.

Before quantifying these metrics, we analyze the shipments first. Figure 5 shows the time-varying air temperature profile as input for the physics-based simulations. The shipments showed a considerable variation in air temperature and length of time (Figure 5A), which spanned between 19 and 50 days, with more than 35% of the shipments above the median of 31 days (Figure 5B). The cumulative consequence of these factors resulted in a unique cooling history for each shipment.

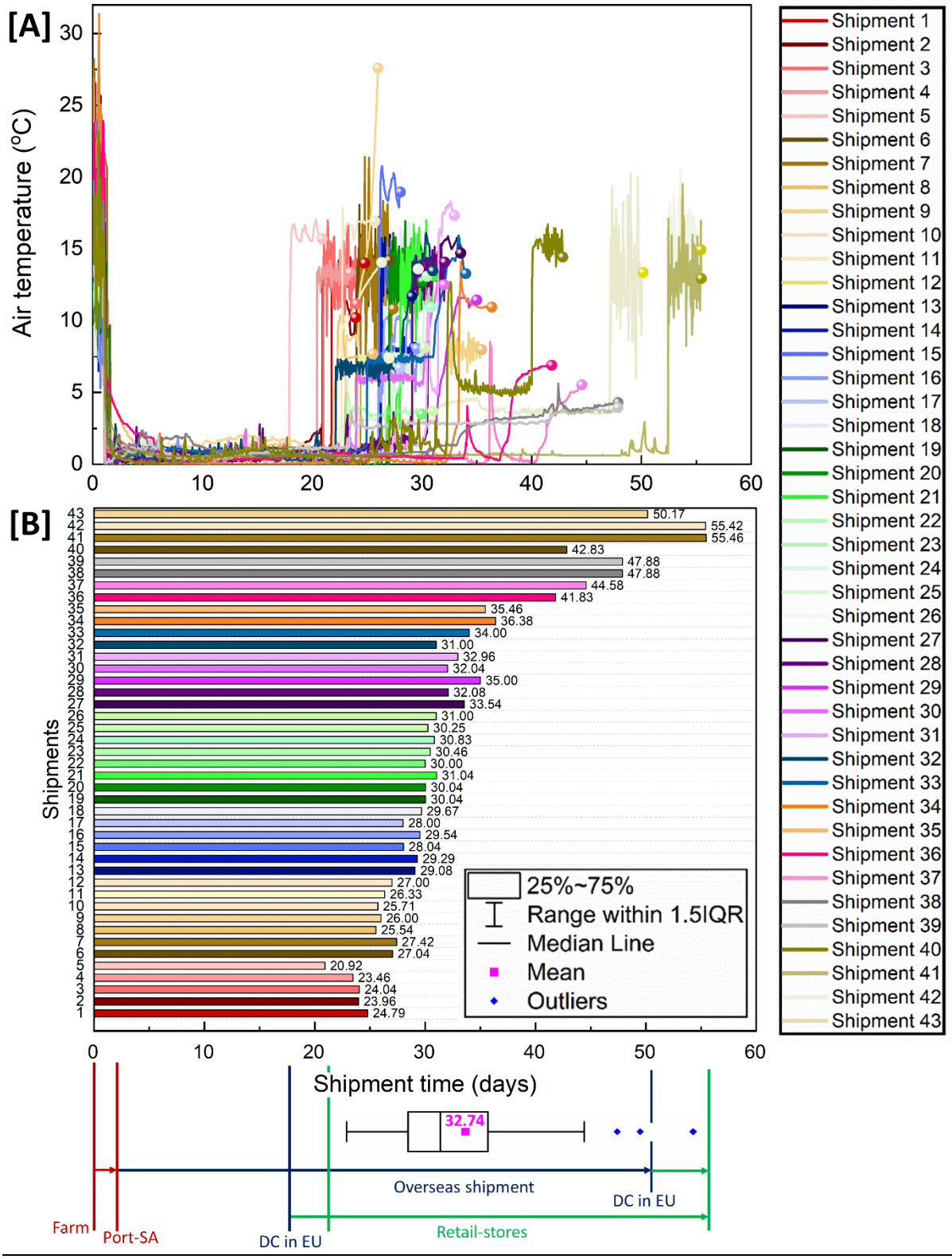

Figure 5. [A] Delivery air temperature as a function of time, as measured by a sensor in 43 different orange shipments, [B] Corresponding shipment duration. The boxplots within represent the median (centre line), 75th upper and 25th lower quartiles (box limits), and 1.5× the interquartile range (whiskers) (IQR). The farm – port SA corresponds 0 – 2 shipment days; Overseas shipment to distribution center (DC) in Europe (EU) corresponds 3 – 19, up to 50 shipment days depending on the shipment; Depending on the shipment, retail stores corresponds to 19 – 21 shipment days, and goes up to 55 shipment days.

We first show the impact of hygrothermal variability between shipments on the mass loss evolution of 'Valencia' oranges during their postharvest journey (Figure 6A). The mass loss increased from 0% to 5.6% over shipment time, depending on the shipment air temperature (Figure 6A(i)). This implies that delivery air temperature fluctuations have a major effect on mass loss, as also reported by [15]. The further increase in mass loss after overseas shipment (from distribution center to retail stores) is due to the relatively high temperature and low prevailing ambient relative humidity at retail stores. Figure 6A(ii) shows the large variability of mass loss (2 – 6%) between different shipments at retail, with more than 55% of the shipments having mass loss above 3%. This is significant as the average mass loss of all shipments is 3.3% upon arrival at retail.

We quantify the impact of hygrothermal variability between shipments on the fruit quality index of 'Valencia' oranges during their postharvest journey (Figure 6B). The fruit quality index decreased with shipment time for all shipments (Figure 6B(i)). The fruit quality index between different shipments at retail varies between 20 to 43% (Figure 6B(ii)). The very high variability of over 20% signifies that more than 60% of the shipments (about 26 shipments) contain fruits of significantly different quality upon arrival at the retail. This remarkable insight is echoed in the remaining shelf life days between fruits of different shipments at retail. The average remaining shelf life of the shipment was 6 days, and the standard deviation was 2.4 days. The min and max values were 0.0 and 8.9 days, respectively. This means that some shipments arrived at the retail with oranges that must be consumed immediately or within 9 days to avoid losses.

The impact of postharvest variability on the chilling injury of oranges during shipment is shown in Figure 7A. Chilling injury severity increased from 0 to ~17% with increasing shipment time for different shipments (Figure 7A (i)). The difference in chilling injury severity between shipments during transit is up to 10%. The temperature fluctuation or deviation from the target air temperature (-1°C or 0 °C) is responsible for the large variation in the chilling injury between different shipments. Increasing the temperatures above a threshold chilling inducing temperature (>4 °C) could increase the fruit tolerance due to gradual conditioning. Figure 7A (ii) shows that the mean chilling injury at retail is 5%, and the variability between shipments is ~5%. This means that all shipments contain fruits with different levels of chilling injury severity upon arrival at retail. In fact, ~20% of the shipments contain fruits with chilling injury above the severe commercial threshold at retail.

We also evaluate the impact of postharvest variability on the evolution of MFF mortality during shipment (Figure 7B). The mean effective lethality at 2 °C for all the shipments was found to be 14 days, which is less than the targeted 16.7 days (Figure 7B (i)). This means that all shipments attained MFF mortality of more than 99.9968% during transit, which is above the required Probit-9 treatment recommended by phytosanitary protocols [56]. Thus, variability between shipments does not have an impact on MFF mortality. This can be further observed in Figure 7B(ii), with all shipments having 100% MFF mortality at the end of the supply chain.

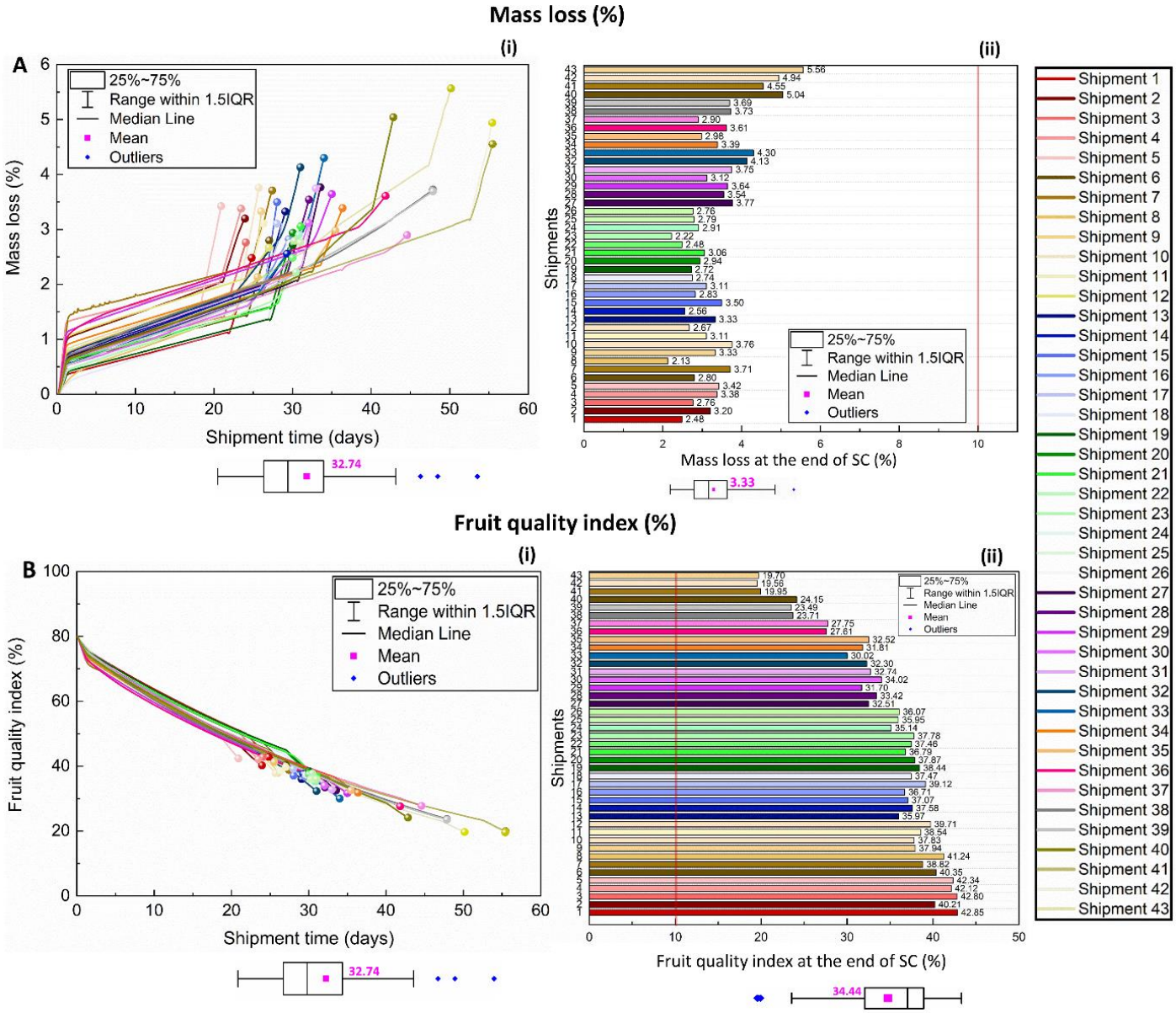

Figure 6. Digital twin output for [A] mass loss, and [B] fruit quality index (%) of oranges for different shipments across their postharvest supply chain. The initial fruit quality of 80% was assumed when leaving the packhouse calibrated based on measured quality data. The colored balls in (i) signify the end of each shipment. The boxplots represent the median (centre line), 75th upper and 25th lower quartiles (box limits) and 1.5× the interquartile range (IQR, whiskers). SC = supply chain. The red-colored vertical line in plots (ii) signifies the threshold value for the different quality metrics

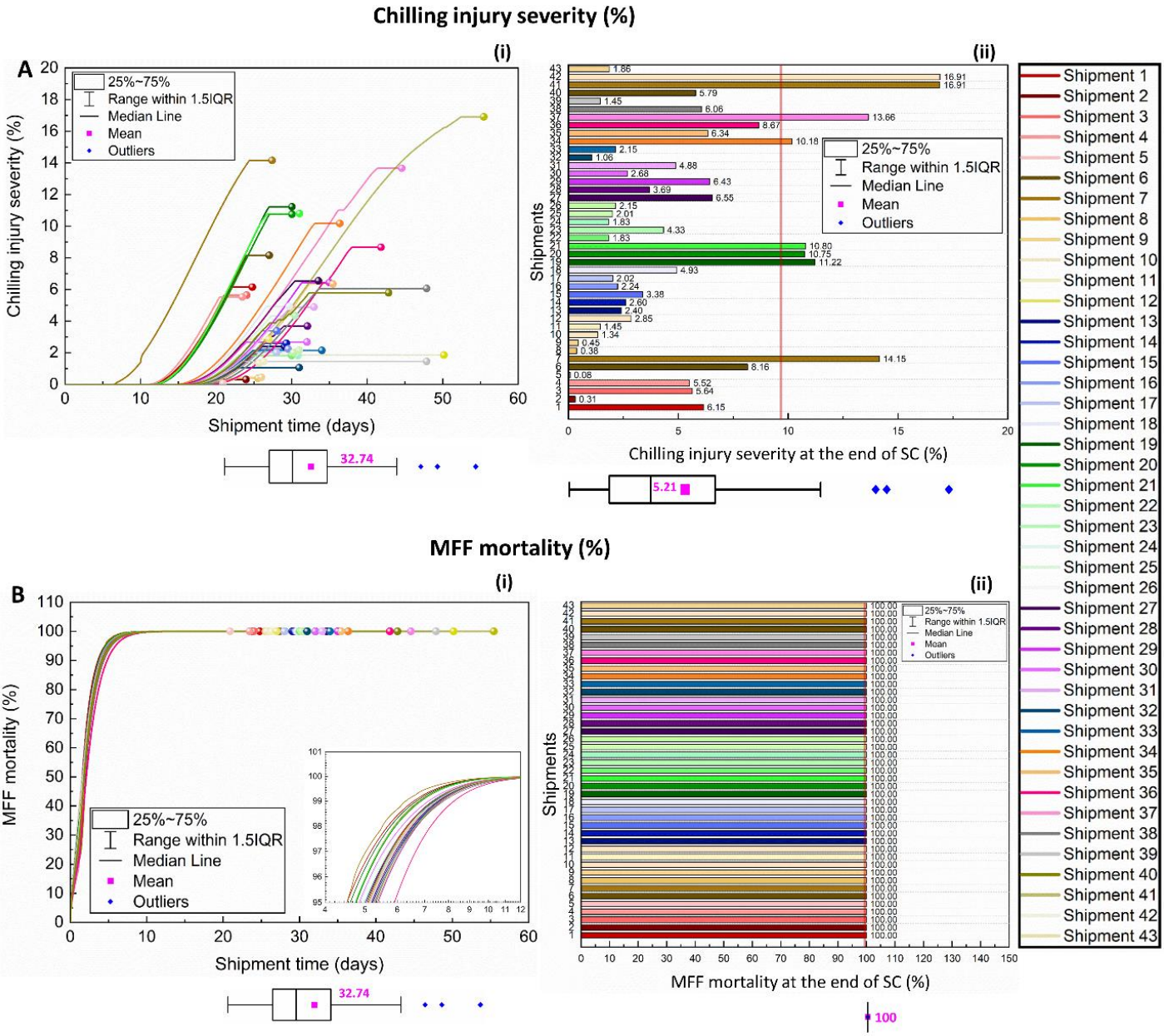

Figure 7. Digital twin output for [A] chilling injury severity (%) and [B] Mediterranean fruit fly (MFF) mortality (%) of oranges for different shipments across their postharvest supply chain. The initial fruit quality of 80% was assumed when leaving the packhouse calibrated based on measured quality data. The colored balls in (i) signify the end of each shipment. The boxplots represent the median (centre line), 75th upper and 25th lower quartiles (box limits) and 1.5× the interquartile range (IQR, whiskers). SC = supply chain. The red-colored vertical line in plots (ii) signifies the threshold value for the different quality metrics.

3.4 Comparison between the impact of pre- and postharvest variability on the quality evolution of orange fruit

The variability in end quality upon arrival due to (1) pre-harvest biological variability in fruit properties and (2) postharvest variability in hygrothermal conditions in the supply chain of 'Valencia' orange fruits were compared. We used a probability distribution function and rug plot as shown in Figure 8. Here, we only included actionable metrics of which both pre-harvest and postharvest variability have a significant impact during shipment. In Figure 8A, we see that the variability in the mass loss at the end of the supply chain is caused, to a similar extent, by the inherent variability in fruit properties after harvest and by the variability in hygrothermal storage conditions during transit. Both pre-harvest and postharvest variability significantly impact the fruit quality index and remaining shelf life days at retail (Figures 8B and 8C). Nevertheless, postharvest variability induces a slightly larger spread in the final quality and remaining shelf life days.

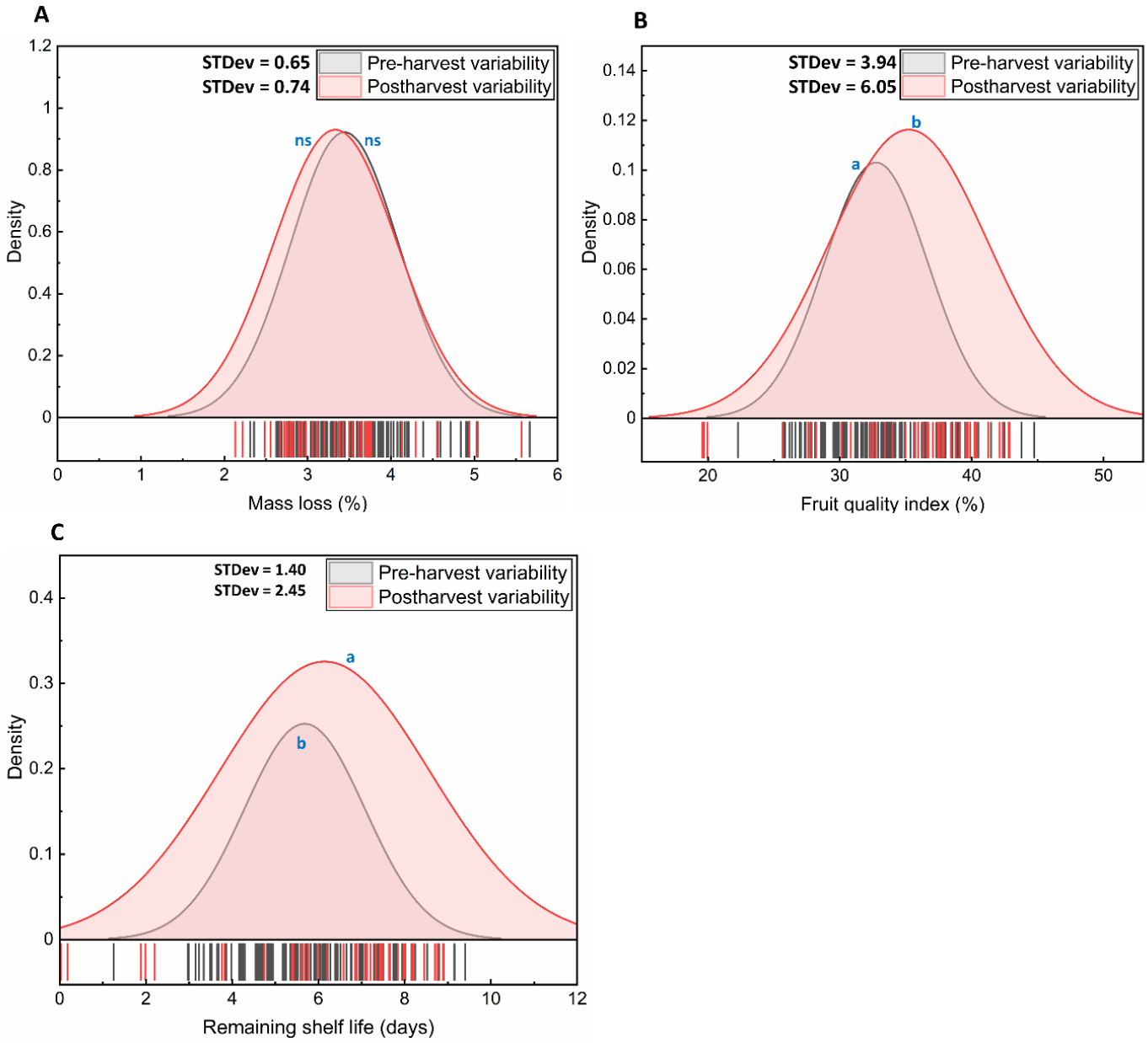

Figure 8. A comparison between the impact of pre-harvest biological variability and postharvest variability on [A] mass loss (%), [B] fruit quality index (%), and [C] remaining shelf life (days) at the end of supply chain using a probability distribution function and rug plot. The rug plot shows the actual data set used for the STDev = standard deviation between groups. Two sample t-test with equal variance assumed at $p \leq 0.05$ significant level was used to compare the mean significant difference of quality evolution due to pre-harvest biological variability and cold chain variability at the end of the supply chain. They are indicated with letters a and b for statistically significantly different groups and ns for not statistically significant groups.

4 CONCLUSIONS

The knowledge of when, where and why food loss occurs in the supply chain of fruits is the first step to unraveling the currently uncharted and invisible quality losses in fresh produce. The following key points well summarize our study:

- For a single shipment, we found variability in the mass loss between individual fruit at retail of up to 1.2%. We found that about 20% of the fruits in a shipment upon arrival at retail are of significantly different fruit quality. The variability in the remaining shelf life of several days exists between individual fruits. This means that the fruits the consumers buy could last for different days, which is a challenge for the retailers to further ensure consumer satisfaction. Our findings also show that a single shipment upon arrival at the retail is without pest infestation.

- Concerning multiple shipments, we found that more than 90% of shipments have high varying fruit mass loss upon arrival at retail. More than 60% of these shipments contain fruits of significantly different fruit quality at retail. The remaining shelf life of the fruits that the consumer buys from the retailer differs by up to 3 days. This complicates supply and demand in the citrus supply chain. Our findings also show that about 20% of shipments contain fruits with chilling injury above the severe commercial threshold at retail. This means that the retailer could throw away 20% of the fruits they receive, which also translates into a significant loss in income.

- Both pre-harvest (STDev = 0.65) and postharvest variability in hygrothermal conditions (STDev = 0.74) causes high varying mass loss in oranges upon arrival at retail. Compared to pre-harvest biological variability in fruit properties (STDev = 3.94), the postharvest variability (STDEV = 6.05) results in more oranges with significantly different quality at retail. The postharvest variability leads to slightly more variations in the remaining shelf life (3 days) of oranges at retail compared to pre-harvest variability (2 days).

This simulation-based research has enabled us to address a key issue in postharvest supply chains: Where does the variability in end quality upon arrival, which many stakeholders regularly observe, come from? We unveiled the extent to which biological variability after harvest between different fruit and the variability in hygrothermal storage conditions between different shipments causes non-uniform end quality.

Acknowledgments

The first author is grateful to Empa for providing the financial resources to conduct this research. We are also thankful to Dr. Tim Grout and Dr. Vaughan Hattingh for their valuable comments and suggestions.

AUTHOR CONTRIBUTIONS

DIO: Conceptualization, Methodology, Investigation, Project administration, Writing-Original draft, Review & Editing. **CS:** Methodology, Review & Editing. **FB:** Bayesian statistics, Review & Editing. **SS:** Review & Editing. **EC:** Review & Editing. **KS:** Review & Editing. **PC**: Review & Editing. **TB:** Review and Editing. **JN:** Review & Editing. **NK:** Review & Editing. **TD**: Conceptualization, Methodology, Supervision, Project administration, Review & Editing.

REFERENCES

[1] L. G. Bellù, “Food losses and waste: Issues and policy options,” no. September, p. 18, 2017.
[2] J. Gustavsson, C. Cederberg, S. Ulf, R. van Otterdijk, and A. Meybeck, “Global Food loss and food waste: Extent, Causes and solutions,” Rome, 2011.
[3] E. Cassou *et al.*, “Nigeria Food Smart Country Diagnostic,” 2020.
[4] T. Garnett, “Fruit and Vegetables & Uk Greenhouse Gas Emissions : Exploring the Relationship Working Paper Produced As Part of the Work of the Food Climate,” *Food Clim. Res. Netw.*, pp. 1–134, 2006.
[5] I. Lake *et al.*, “Food and Climate change: A review of the effects of climate change on food within the remit of the Food Standards Agency,” *Food Clim. Rep.*, pp. 1–111, 2015.
[6] P. J. R. Cronje, J. Joubert, H. Marais, E. W. Hoffman, and L. Zacarías, “Influence of late nitrogen soil applications on mandarin fruit quality,” *Citrus Res. Technol.*, vol. 37, no. 1, pp. 56–65, 2016, doi: 10.4322/crt.icc081.
[7] J. Lado *et al.*, “Light Regulation of Carotenoid Biosynthesis in the Peel of Mandarin and Sweet Orange Fruits,” *Front. Plant Sci.*, vol. 10, no. October, pp. 1–16, 2019, doi: 10.3389/fpls.2019.01288.
[8] M. S. Sibomana, T. S. Workneh, and K. Audain, “A review of postharvest handling and losses in the fresh tomato supply chain: a focus on Sub-Saharan Africa,” *Food Secur.*, vol. 8, no. 2, pp. 389–404, 2016, doi: 10.1007/s12571-016-0562-1.
[9] L. Di Vittori, L. Mazzoni, M. Battino, and B. Mezzetti, “Pre-harvest factors influencing the quality of berries,” *Sci. Hortic. (Amsterdam).*, vol. 233, no. July 2017, pp. 310–322, 2018, doi: 10.1016/j.scienta.2018.01.058.
[10] R. Lufu, A. Ambaw, and U. L. Opara, “Water loss of fresh fruit: Influencing pre-harvest, harvest and postharvest factors,” *Sci. Hortic. (Amsterdam).*, vol. 272, no. January, 2020, doi: 10.1016/j.scienta.2020.109519.
[11] D. I. Onwude, G. Chen, N. Eke-emezie, A. Kabutey, A. Y. Khaled, and B. Sturm, “Recent Advances in Reducing Food Losses in the Supply Chain of Fresh Agricultural Produce,” *Processes*, vol. 8, no. 11, p. 1431, Nov. 2020, doi: 10.3390/pr8111431.
[12] S. Mercier, S. Villeneuve, M. Mondor, and I. Uysal, “Time–Temperature Management Along the Food Cold Chain: A Review of Recent Developments,” *Compr. Rev. Food Sci. Food Saf.*, vol. 16, no. 4, pp. 647–667, 2017, doi: 10.1111/1541-4337.12269.
[13] M. L. A. T. M. Hertog, N. Scheerlinck, and B. M. Nicolaï, “Monte Carlo evaluation of biological variation: Random generation of correlated non-Gaussian model parameters,” *J. Comput. Appl. Math.*, vol. 223, no. 1, pp. 1–14, 2009, doi: 10.1016/j.cam.2007.12.010.
[14] K. Joshi, J. Warby, J. Valverde, B. Tiwari, P. J. Cullen, and J. M. Frias, “Impact of cold chain and product variability on

quality attributes of modified atmosphere packed mushrooms (Agaricus bisporus) throughout distribution," *J. Food Eng.*, vol. 232, pp. 44–55, 2018, doi: 10.1016/j.jfoodeng.2018.03.019.

[15] K. Joshi, B. Tiwari, P. J. Cullen, and J. M. Frias, "Predicting quality attributes of strawberry packed under modified atmosphere throughout the cold chain," *Food Packag. Shelf Life*, vol. 21, no. June, p. 100354, 2019, doi: 10.1016/j.fpsl.2019.100354.

[16] M. L. A. T. M. Hertog, J. Lammertyn, M. Desmet, N. Scheerlinck, and B. M. Nicolaï, "The impact of biological variation on postharvest behaviour of tomato fruit," *Postharvest Biol. Technol.*, vol. 34, no. 3, pp. 271–284, 2004, doi: 10.1016/j.postharvbio.2004.05.014.

[17] S. Duret *et al.*, "Identification of the significant factors in food quality using global sensitivity analysis and the accept-and-reject algorithm. Part III: Application to the apple cold chain," *J. Food Eng.*, vol. 148, pp. 66–73, 2015, doi: 10.1016/j.jfoodeng.2014.09.039.

[18] S. G. Gwanpua, V. Vicent, B. E. Verlinden, M. L. A. T. M. Hertog, B. M. Nicolai, and A. H. Geeraerd, "Managing biological variation in skin background colour along the postharvest chain of 'Jonagold' apples," *Postharvest Biol. Technol.*, vol. 93, pp. 61–71, 2014, doi: 10.1016/j.postharvbio.2014.02.008.

[19] M. L. A. T. M. Hertog, N. Scheerlinck, J. Lammertyn, and B. M. Nicolaï, "The impact of biological variation on postharvest behaviour of Belgian endive: The case of multiple stochastic variables," *Postharvest Biol. Technol.*, vol. 43, no. 1, pp. 78–88, 2007, doi: 10.1016/j.postharvbio.2006.07.007.

[20] K. Shoji, S. Schudel, D. Onwude, C. Shrivastava, and T. Defraeye, "Resources , Conservation & Recycling Mapping the postharvest life of imported fruits from packhouse to retail stores using physics-based digital twins," *Resour. Conserv. Recycl.*, vol. 176, p. 105914, 2022, doi: 10.1016/j.resconrec.2021.105914.

[21] T. Defraeye *et al.*, "Digital twins are coming: Will we need them in supply chains of fresh horticultural produce?," *Trends Food Sci. Technol.*, vol. 109, no. March 2020, pp. 245–258, 2021, doi: 10.1016/j.tifs.2021.01.025.

[22] P. Verboven, T. Defraeye, A. K. Datta, and B. Nicolai, "Digital twins of food process operations: the next step for food process models?," *Curr. Opin. Food Sci.*, vol. 35, pp. 79–87, 2020, doi: 10.1016/j.cofs.2020.03.002.

[23] D. Ivanov and A. Dolgui, "A digital supply chain twin for managing the disruption risks and resilience in the era of Industry 4.0," *Prod. Plan. Control*, vol. 0, no. 0, pp. 1–14, 2020, doi: 10.1080/09537287.2020.1768450.

[24] RStudio Team, "RStudio: Integrated Development for R," *RStudio, PBC, Boston, MA*, 2020. [Online]. Available: http://www.rstudio.com/.

[25] L. L. Goedhals-Gerber and G. Khumalo, "Identifying temperature breaks in the export cold chain of navel oranges: A Western Cape case," *Food Control*, vol. 110, no. December, 2020, doi: 10.1016/j.foodcont.2019.107013.

[26] V. Goulas and G. A. Manganaris, "Exploring the phytochemical content and the antioxidant potential of Citrus fruits grown in Cyprus," *Food Chem.*, vol. 131, no. 1, pp. 39–47, 2012, doi: 10.1016/j.foodchem.2011.08.007.

[27] J. Bai *et al.*, "Changes in volatile and non-volatile flavor chemicals of 'valencia' orange juice over the harvest seasons," *Foods*, vol. 5, no. 1, pp. 1–17, 2016, doi: 10.3390/foods5010004.

[28] S. Khalid, A. U. Malik, B. A. Saleem, A. S. Khan, M. S. Khalid, and M. Amin, "Tree age and canopy position affect rind quality, fruit quality and rind nutrient content of 'Kinnow' mandarin (Citrus nobilis Lour×Citrus deliciosa Tenora)," *Sci. Hortic. (Amsterdam).*, vol. 135, pp. 137–144, 2012, doi: 10.1016/j.scienta.2011.12.010.

[29] M. Rehman, Z. Singh, and T. Khurshid, "Methyl jasmonate alleviates chilling injury and regulates fruit quality in 'Midknight' Valencia orange," *Postharvest Biol. Technol.*, vol. 141, no. March, pp. 58–62, 2018, doi: 10.1016/j.postharvbio.2018.03.006.

[30] B. R. Becker, A. Misra, and B. A. Fricke, "Bulk refrigeration of fruits and vegetables part I: Theoretical considerations of heat and mass transfer," *HVAC R Res.*, vol. 2, no. 2, pp. 122–134, 1996, doi: 10.1080/10789669.1996.10391338.

[31] M. J. Ferrua and R. P. Singh, "Modeling the forced-air cooling process of fresh strawberry packages, Part I: Numerical model," *Int. J. Refrig.*, vol. 32, no. 2, pp. 335–348, 2009, doi: 10.1016/j.ijrefrig.2008.04.010.

[32] W. Wu and T. Defraeye, "Identifying heterogeneities in cooling and quality evolution for a pallet of packed fresh fruit by using virtual cold chains," *Appl. Therm. Eng.*, vol. 133, pp. 407–417, 2018, doi: 10.1016/j.applthermaleng.2017.11.049.

[33] J. Dehghannya, M. Ngadi, and C. Vigneault, "Mathematical Modeling Procedures for Airflow, Heat and Mass Transfer During Forced Convection Cooling of Produce: A Review," *Food Eng. Rev.*, vol. 2, no. 4, pp. 227–243, 2010, doi: 10.1007/s12393-010-9027-z.

[34] G. Tagliavini, T. Defraeye, and J. Carmeliet, "Multiphysics modeling of convective cooling of non-spherical, multi-material fruit to unveil its quality evolution throughout the cold chain," *Food Bioprod. Process.*, vol. 117, pp. 310–320, 2019, doi: 10.1016/j.fbp.2019.07.013.

[35] S. Whitaker, "Forced convection heat transfer correlations for flow in pipes, past flat plates, single cylinders, single spheres, and for flow in packed beds and tube bundles," *AIChE J.*, vol. 18, no. 2, pp. 361–371, Mar. 1972, doi: 10.1002/aic.690180219.

[36] C. Cogné, P. U. Nguyen, J. L. Lanoisellé, E. Van Hecke, and D. Clausse, "Modeling heat and mass transfer during vacuum freezing of puree droplet," *Int. J. Refrig.*, vol. 36, no. 4, pp. 1319–1326, 2013, doi: 10.1016/j.ijrefrig.2013.02.003.

[37] ASHRAE, *Ashrae Handbook- Refrigeration: Systems and Applications*. Atlanta, 2018.

[38] M. Ladaniya, "Storage systems and response of citrus fruits," *Citrus Fruit Biol. Technol. Eval. Citus fruit*, pp. 333–373, 2008.

[39] G. L. Robertson, *Food Packaging: Principles and Practice, Third Edition*, Third. Boca-Raton: Taylor & Francis Group LLC, 2016.

[40] M. A. J. S. Van Boekel, "Kinetic modeling of food quality: A critical review," *Compr. Rev. Food Sci. Food Saf.*, vol. 7, pp. 144–158, 2008, doi: 10.1111/j.1541-4337.2007.00036.x.

[41] K. J. Valentas, E. Rotstein, and R. P. Singh, *Handbook of food engineering practice*. CRC Press, 1997.

[42] J. L. Zaragozá, "La UE ha detectado casi 140 envíos de cítricos importados de Sudáfrica con plagas desde 2015 - Levante-EMV," *Levante-EMV*, 2019.

[43] Animal and Plant Health Inspection Service, "Federal Register: Importation of Fresh Citrus Fruit From the Republic of South Africa Into the Continental United States," 2014.

[44] P. Biswas, A. R. East, E. W. Hewett, and J. A. Heyes, "Chilling injury in tomato fruit," *Hortic. Rev. (Am. Soc. Hortic. Sci).*, vol. 44, pp. 229–278, 2016.

[45] E. Chalutz, J. Waks, and M. Schiffmann-Nadel, "A comparison of the response of different citrus fruit cultivars to storage temperature," *Sci. Hortic. (Amsterdam).*, vol. 25, no. 3, pp. 271–277, 1985, doi: 10.1016/0304-4238(85)90125-6.

[46] A. R. Moritz and F. C. Henriques, "Studies of Thermal Injury: II. The Relative Importance of Time and Surface Temperature in the Causation of Cutaneous Burns," *Am. J. Pathol.*, vol. 23, no. 5, pp. 695–720, Sep. 1947.

[47] D. Holcroft, "Water Relations in Harvested Fresh Produce," *Postharvest Educ. Found. White Pap.*, no. 15, pp. 1–16, 2015.

[48] J. F. Thompson, F. G. Mitchell, and T. R. Rumsay, *Commercial Cooling of Fruits, Vegetables, and Flowers*. University of California, Agriculture and Natural Resources, 2008.

[49] T. Defraeye *et al.*, "Digital twins probe into food cooling and biochemical quality changes for reducing losses in refrigerated supply chains," *Resour. Conserv. Recycl.*, vol. 149, no. August, pp. 778–794, 2019, doi: 10.1016/j.resconrec.2019.06.002.

[50] X. I. Siboza, I. Bertling, and A. O. Odindo, "Enzymatic antioxidants in response to methyl jasmonate and salicylic acid and their effect on chilling tolerance in lemon fruit [Citrus limon (L.) Burm. F.]," *Sci. Hortic. (Amsterdam).*, vol. 225, no. July, pp. 659–667, 2017, doi: 10.1016/j.scienta.2017.07.023.

[51] S. Musacchi and S. Serra, "Apple fruit quality: Overview on pre-harvest factors," *Sci. Hortic. (Amsterdam).*, vol. 234, no. December 2017, pp. 409–430, 2018, doi: 10.1016/j.scienta.2017.12.057.

[52] Y. Kashash, L. Mayuoni-Kirshenbaum, L. Goldenberg, H. J. Choi, and R. Porat, "Effects of harvest date and low-temperature conditioning on chilling tolerance of 'Wonderful' pomegranate fruit," *Sci. Hortic. (Amsterdam).*, vol. 209, pp. 286–292, 2016, doi: 10.1016/j.scienta.2016.06.038.

[53] National Department of Agriculture, "Import Requirements for Fresh Citrus (Orange , Lemon , Grapefruit) from South Africa," 2018.

[54] C. P. F. De Lima, A. J. Jessup, L. Cruickshank, C. J. Walsh, and E. R. Mansfield, "Cold disinfestation of citrus (Citrus spp.) for mediterranean fruit fly (ceratitis capitata) and queensland fruit fly (Bactrocera tryoni) (Diptera: Tephritidae)," *New Zeal. J. Crop Hortic. Sci.*, vol. 35, no. 1, pp. 39–50, 2007, doi: 10.1080/01140670709510166.

[55] T. G. Grout *et al.*, "Cold susceptibility and disinfestation of bactrocera invadens (Diptera: Tephritidae) in oranges," *J. Econ. Entomol.*, vol. 104, no. 4, pp. 1180–1188, 2011, doi: 10.1603/EC10435.

[56] FAO and IPPC, "PT 24: Cold treatment for Ceratitis capitata on Citrus sinensis," 2017.

[57] USDA, "Treatment manual," 2002.

[58] PPECB, "Procedure For In-Transit Cold Treatment To Eradicate Fruit Flies In Apples And Pears Shipped From South African Ports To The United States of America," 2010.

[59] ASHRAE, "Air-Cooling and Dehumidifying Coils," in *ASHRAE Handbook- HVAC Applications*, Atlanta: ASHRAE, 2016.

[60] United States. Department of the Air Force, "Refrigerating effect," in *Cold Storage Warehouses* , vol. 88, 1955, pp. 84–86.

[61] J. F. Thompson, F. G. Mitchell, and T. R. Rumsay, *Commercial cooling of fruits, vegetables, and flowers*. University of California, Agriculture and Natural Resources, 2008.

[62] M. C. do N. Nunes, *Color atlas of postharvest quality of fruits and vegetables*. John Wiley & Sons., 2008.

[63] J. F. Thompson, "Pre-cooling and storage facilities," in *USDA Agriculture Handbook Number 66: The Commercial Storage of Fruits, Vegetables, and Florist and Nursery Stocks*, USDA, Ed. USDA, 2004, pp. 1–10.

[64] M. L. L. Jomori, N. D. Berno, and R. A. Kluge, "Aplicação de etileno após o armazenamento refrigerado melhora a coloração de laranja 'Valência," *Rev. Bras. Frutic.*, vol. 38, no. 4, 2016, doi: 10.1590/0100-29452016636.

[65] B. Saberi, J. B. Golding, S. Chockchaisawasdee, C. J. Scarlett, and C. E. Stathopoulos, "Effect of Biocomposite Edible Coatings Based on Pea Starch and Guar Gum on Nutritional Quality of 'Valencia' Orange During Storage," *Starch / Staerke*, vol. 70, no. 5–6, pp. 1–10, 2018, doi: 10.1002/star.201700299.

[66] C. M. C. Yuen, N. O. Tridjaja, R. B. H. Wills, and B. L. Wild, "Chilling injury development of 'Tahitian' lime, 'Emperor' mandarin, 'Marsh' grapefruit and 'Valencia' orange," *J. Sci. Food Agric.*, vol. 67, no. 3, pp. 335–339, 1995, doi: https://doi.org/10.1002/jsfa.2740670310.

[67] P. L. Davis and C. Hofmann, "Reduction of Chilling Injury of Citrus Fruits in Cold Storage by Intermittent Warming," *J. Food Sci.*, vol. 38, pp. 871–873, 1973.

[68] Y. F. Jin, Z. Y. Yin, W. H. Zhou, and S. Horpibulsuk, "Identifying parameters of advanced soil models using an enhanced transitional Markov chain Monte Carlo method," *Acta Geotech.*, vol. 14, no. 6, pp. 1925–1947, 2019, doi: 10.1007/s11440-019-00847-1.

[69] F. Korner-Nievergelt, T. Roth, S. von Felten, J. Guélat, B. Almasi, and P. Korner-Nievergelt, "Markov Chain Monte Carlo Simulation," *Bayesian Data Anal. Ecol. Using Linear Model. with R, BUGS, STAN*, pp. 197–212, 2015, doi: 10.1016/b978-0-12-801370-0.00012-5.

[70] S. E. Jorgensen, "Fundamentals of ecological modelling," *Oceanogr. Lit. Rev.*, vol. 9, no. 42, pp. 759–760, 1995.

[71] M. Quinet *et al.*, "Tomato Fruit Development and Metabolism," *Front. Plant Sci.*, vol. 10, no. November, pp. 1–23, 2019, doi: 10.3389/fpls.2019.01554.
[72] A. K. Cowan, R. F. Cripps, E. W. Richings, and N. J. Taylor, "Fruit size: Towards an understanding of the metabolic control of fruit growth using avocado as a model system," *Physiol. Plant.*, vol. 111, no. 2, pp. 127–136, 2001, doi: 10.1034/j.1399-3054.2001.1110201.x.
[73] R. C. O. Okello *et al.*, "A multilevel analysis of fruit growth of two tomato cultivars in response to fruit temperature," *Physiol. Plant.*, vol. 153, no. 3, pp. 403–418, 2015, doi: 10.1111/ppl.12247.
[74] M. Zekri, "Factors affecting citrus production and quality," *Citrus Ind.*, no. December, pp. 1–6, 2011.
[75] S. Sharma, K. Barman, M. W. Siddiqui, and V. Nath, *Training and Pruning for Improved Postharvest Fruit Quality*. Elsevier Inc., 2018.

SUPPLEMENTARY MATERIAL

1. Measurement of air temperature during shipment

The temperature data logger used to measure the air temperature of fruits during shipments was TempTale®4 (TT4) GEO Eagle Extended (SENSITECH, Beverly, MA, USA). This sensor has an accuracy of ±0.5 °C and logged the air temperature every 60 minutes. For most shipments, only air temperature were measured, as these are required by the export guidelines.

Every shipment was equipped with five sensors in accordance with the prescribed export guidelines. Of these, two sensors recorded the temperature of the air delivered to and returning from the cargo space. The other three sensors recorded the fruit pulp temperature at three critical locations in the cargo. The sensors placed in the three locations, namely USDA1, USDA2 and USDA3 (see Figure S1). These are usually fixed locations in the container, as they are defined by USDA regulations [57], [58].

- USDA1 is in the fruit in the top of the first pallet on the left-hand side of the container, close to the centre line of the container.
- USDA2 is placed into the fruit within a pallet in the middle of the container at half height and close to the centre line of the container.
- USDA3 is placed in the second last row of pallets from the door on the left-hand side of the container at half height of the pallet.

In this study, we used mainly datasets for the air temperature measured in USDA3.

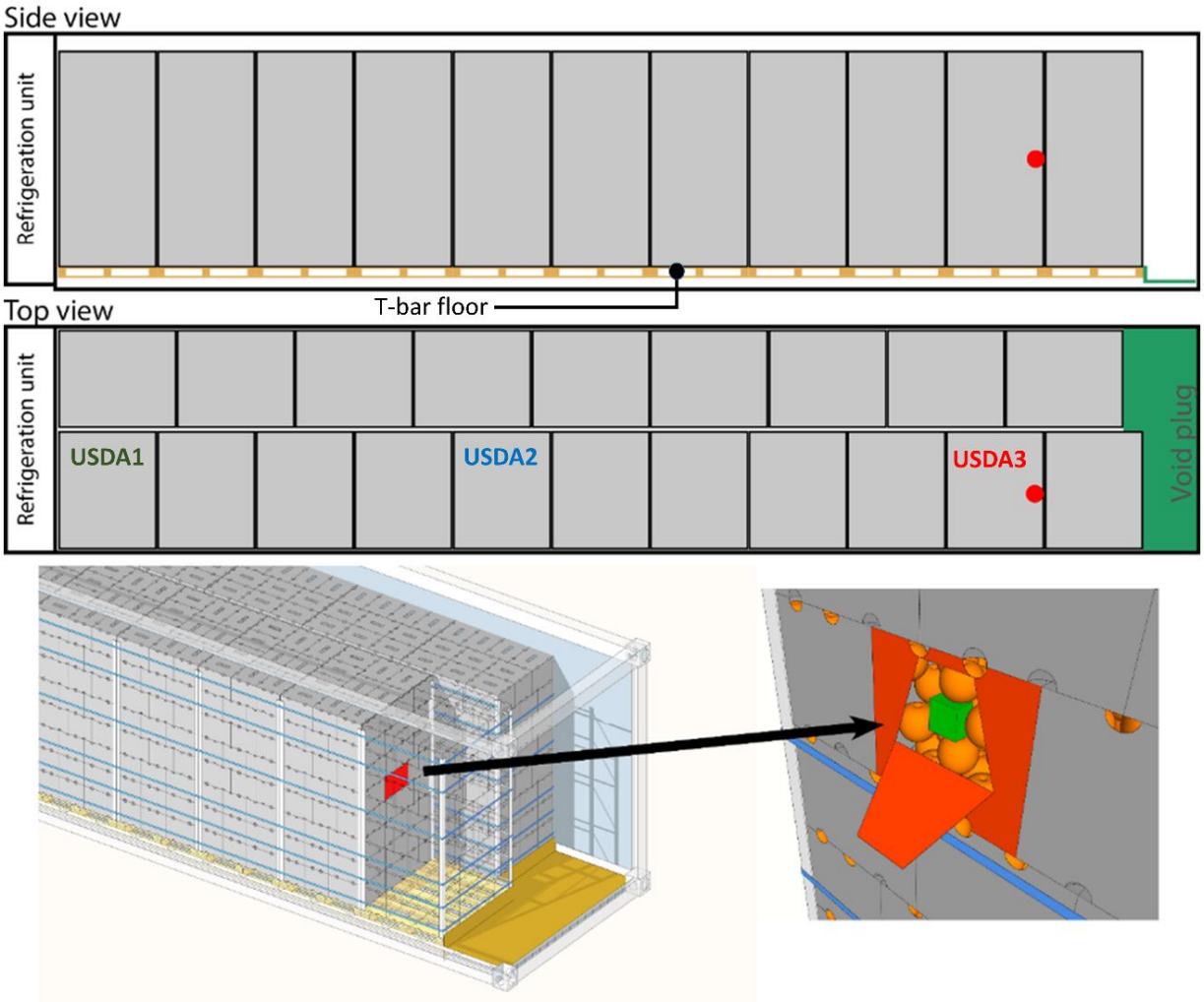

Figure S1. *Side and top cross-sectional views of a refrigerated container with an indication of sensor placement.*

2. Thermal model

Heat of respiration

The heat of respiration was estimated from a correlation between the carbon dioxide production rate of oranges and it's temperature as expressed in Equation S1[30]:

$$\dot{m}_{CO_2} = f.\left(\frac{9T}{5} + 32\right)^{g} \quad (S1)$$

where $\dot{m}_{CO_2}$ is the carbon production rate per unit mass of orange (mg.kg^{-1} h^{-1}), T is the average commodity temperature (^{o}C), and f (2.81 x 10^{-4}) and g (2.68) are respiration coefficients for oranges [30].

Actual airspeed around the fruit

We used Equation 3 to estimate the actual airspeed around orange fruit. The porosity in a pallet of orange fruits (ϕ) was 39%. This corresponds to the fraction of void volume (volume occupied by air) with respect to the total volume of the porous medium (volume occupied by air + fruit). Delivery air with a flow rate (Q_{air}) of 4000 m^3·h^{-1}, estimated for general shipping containers, was assumed to enter this porous medium from the bottom of the cargo space. This was used to determine the superficial airspeed ($u_{\text{superficial}}$, m·s^{-1}) using the cross-sectional area of the bottom of the cargo space (A_{cross}, m^2). However, this space-averaged superficial airspeed ($u_{\text{superficial}}$, m·s^{-1}) is different from the speed of the air confined in the porous medium-the void space between the fruits (u_{physical}, m·s^{-1}).

3. Mass loss model

Estimating relative humidity of air

The relative humidity of the air within the refrigerated container (RH_{air}, %) was estimated using the principles of psychrometry, by assuming a constant sensible heat ratio (*SHR*) within the refrigerated container. The *SHR* is a performance characteristic for evaluating the thermodynamic conditions for air in a cold room, and forms the basis for the design of air conditioning systems.

The two reference conditions used to determine this *SHR* were cold storage (-1.5 °C, 95% RH) and ambient (20 °C, 55% RH). The *SHR* was thus calculated to be 0.635 using Equation S2 [59], which also matched with that qualitatively obtained from a psychrometric chart (Figure S2). This implies that 63.5% of the load provided to the room is responsible for cooling the air (sensible load) and 36.5% of the load is responsible for controlling the humidity (latent load). For storage rooms designed for fruits and vegetables, the SHR lies between 0.54 – 0.72 [60].

$$SHR = \frac{c_{p,air}(\mathrm{T_2} - \mathrm{T_1})}{h_2 - h_1} \quad (S2)$$

where $C_{\text{p,air}}$ = 1.005 kJ·kg^{-1}·°K^{-1}, h is the corresponding enthalpy (kJ·kg^{-1}), T_1 and T_2 correspond to the ambient and cold air dry bulb temperature (°C) respectively.

A constant *SHR* (=0.635) was assumed for the air in the refrigerated container. This means that the thermodynamic properties of air entering the refrigerated container will always fall on the red line in Figure S2.

At a given dry bulb temperature (T_{db}, °C), the enthalpy was thus estimated from Equation S1. The enthalpy was used to estimate the absolute humidity Y (kg$_{\text{wv}}$·kg$_{\text{da}}^{-1}$) using Equation S3.

$$h = 1.005T_{db} + Y(1.88T_{db} + 2501) \quad (S3)$$

The vapor pressure for air at a given T_{db} was calculated using the humid ratio as expressed in Equation S4 [61].

$$p_{v,air} = \frac{Y \times P_{atm}}{0.622} \quad (S4)$$

The saturated vapor pressure was calculated using Equation S5, as a function of the dry-bulb air temperature (T_{db}, °C) using the Antoine equation [30].

$$P_{sat} = \exp\left(23.4795 - \frac{3990.5}{T_{air} - 39.317}\right) \quad (S5)$$

The relative humidity of air (RH_{air}, %) was estimated using Equation S6 [61].

$$RH_{air} = \frac{P_{v,air}}{P_{sat}}\ x\ 100 \quad \text{(S6)}$$

Mass transfer coefficient

The mass transfer coefficient (k_{air}) was estimated based on the airspeed (u_{air}, m·s^{-1}) using the Sherwood correlation for a sphere (Equation 7). The base case Sherwood number *(Sh)* for this study is 15.56, resulting in a mass transfer coefficient (k_{air}) of 0.004651 m.s^{-1}. Note that k_{air} (m.s^{-1}) from Equation 7 was finally expressed as a partial differential of the dynamic air temperature (k_{air} s·m^{-1}). The k_{air} (s·m^{-1}) value using the average dynamic air temperature for the base case single shipment (i.e., -1°C targeted delivery cold air temperature and shipment length of 30 days) closely corresponds to the mass transfer coefficient obtained using the heat and mass transfer Chilton-Colburn analogy (i.e., $\frac{K_{air}}{h_c} = 7\ x\ 10^{-9}$).

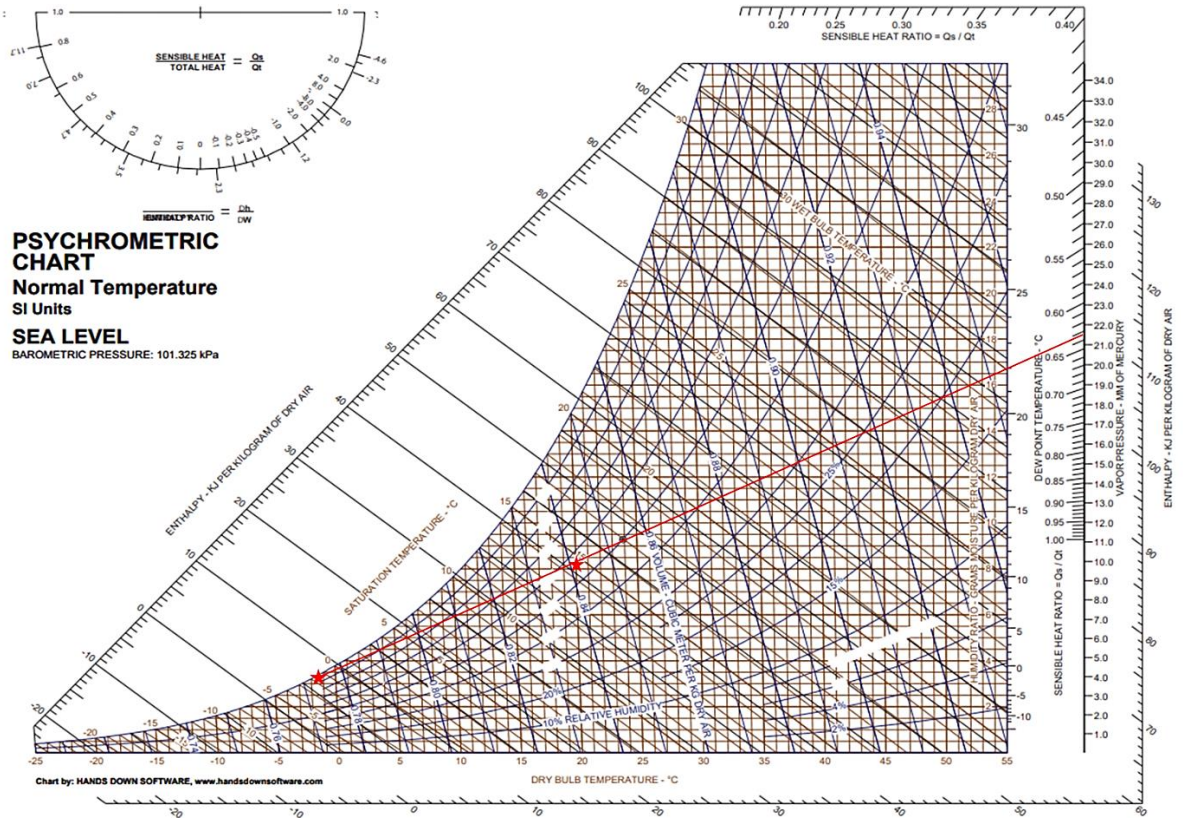

Figure S2: Psychrometric chart showing thermodynamic properties of the air in the refrigerated container as it transitions from ambient conditions (20 °C, 55% RH) to those of cold storage (-1.5 °C, 95% RH). This image is available in the public domain via (https://chbe241.github.io/).

4. Quality model

The quality of citrus fruit varies from one fruit to another in a single batch and also changes between different cold chains. This quality evolution could manifest visually (e.g., changes in appearance) and non-visually (e.g., changes in vitamin C). Most of the underlying biochemical reactions responsible for these quality changes can be adequately modeled, and the evolution of multiple quality attributes such as total soluble solids (TSS [°Brix]), color (Col [scale 1-5]) and fruit quality index ([%]) of the orange fruit predicted.

The fruit quality model was calibrated based on fruit shelflife studies in literature for 'Valencia' oranges [62] and the results of our orange storage experiments (results not shown). Valencia orange can successfully be stored between 32 – 52 days 56 at 0 - 9°C, after which the fruit is considered to be lost [62]. This study assumed 49 shelf life days at 7 °C for the orange quality model calibration. The initial value of the indicator of fruit quality for the base case ($I_{t=0}$) was assumed to be 80% at the start of a shipment (packhouse) (t = 0 s), after calibration with measured field quality data. This is because the fruit has already started to decay from

the point of harvest to the point of sorting and packing at the packhouse, which is the start of shipment for this study. At the end of 49 days period at 7 °C, the fruit reaches the end of its shelf life and the first visual symptoms of decay start to appear. In our calibration, we arbitrarily set this threshold at 10%, a point where the first visual damage occurs and the fruit cannot be sold to the consumer anymore.

To account for the dependence of shelf life on storage temperature, we assumed a Q_{10} factor of 2 (Equation S7). Q_{10} is typically about 2 to 3 for degradation reactions in fruits [39], [63]. A Q_{10} of 2 means that the shelf life of the fruit is halved for every 10 °C rise in storage temperature, so the fruit can be stored for 56 days at 0 °C, 28 days at 10 °C, and 14 days at 20 °C.

$$Q_{10} = \frac{k_{T+10}}{k_T} \tag{S7}$$

which then can be rewritten as follows [40].

$$Q_{10} = \frac{k_{0,i} e^{\frac{-E_{a,i}}{R(T+10)}}}{k_{0,i} e^{\frac{-E_{a,i}}{RT}}} = \frac{e^{\frac{-E_{a,i}}{R(T+10)}}}{e^{\frac{-E_{a,i}}{RT}}} = e^{-E_{a,i}(\frac{1}{R(T+10)} - \frac{1}{RT})} \tag{S8}$$

$$\ln Q_{10} = \frac{10E_{a,i}}{RT(T+10)} \approx \frac{10E_{a,i}}{RT^2} \tag{S9}$$

$$E_{a,i} \approx \frac{RT^2}{10} \ln Q_{10} \tag{S10}$$

With this $E_{a,i}$ value, $k_{0,i}$ was calculated by rearranging Equation 14 and 15 as:

$$k_{0,i} = \frac{k_i(T)}{e^{\frac{-E_{a,i}}{RT}}} = \frac{-\frac{1}{t}\ln(\frac{A_i(t) - C}{A_{0,i}})}{e^{\frac{-E_{a,i}}{RT}}} \tag{S11}$$

where $k_{(T+10)}$, k_T correspond to the rate constants at temperatures (T+*10*) and T [K], respectively. $A_{0,i}$ is the initial overall quality (80%, at t = 0 s), $E_{a,i}$ is the activation energy [J mol^{-1}], R is the ideal gas constant (8.314 J mol^{-1} K^{-1}) and C is an integration constant.

Similarly, the same equations (Equation S7 – S11) were used to calibrate the color and total soluble solids models for 'Valencia' oranges. For color, with a Q_{10} of 2, at a storage temperature of 12 °C, the initial value of -0.6 was assumed at the start of a shipment (t = 0 s), and 0.5 value was assumed at the end of a 30 days shipment based on literature data for 'Valencia orange' [64]. For total soluble solids, we assumed a 28 days storage of 'Valencia' orange at 5 °C, with an initial value of 11.9 °brix (t = 0 s) and a final value of 12.1 °brix based on literature data [65].

5. Lethality model for pest mortality

Equation S12 describes the lethality model using in this study. An equivalent lethality against fruit fly is achieved for the time-temperature treatment maintaining the fruit core temperature at 2 °C for 16.7 days or at 3 °C for 18 days.

$$F_{cumulative,T_{ref}}(\mathrm{t}) = \int_{t=0}^{t=t_{end}} 10^{\left(\frac{T_{ref} - T_{core}(\mathrm{t})}{z}\right)} dt \tag{S12}$$

where T_{core} (t) is the core temperature (K) as a function of time, since here the fruit fly larvae reside and the parameter z corresponds to the z-value (=31.365 K), which accounts for the temperature dependence on the time of exposure. Here, $F_{cumulative,T_{ref}}$ (days) represents the cumulative process lethality, or the equivalent treatment time at the reference temperature (T_{ref}), which is 275.15 K, i.e. 2 °C in our case. $F_{cumulative,T_{ref}}$ was further used to estimate the surviving fraction of MFF at the end of the cold disinfestation treatment using Equation S13.

$$F_{cumulative,T_{ref}} = D_{T_{ref}} \cdot \log\left(\frac{N_0}{N(t)}\right) \tag{S13}$$

Here, D_{Tref} (days) corresponds to the time required to obtain a log reduction of fruit fly at a specific temperature (T_{ref} = 275.15 K). N_0 and $N(t)$ represent the MFF survivors at the start (t=0) and at any time instant (t) of the process, respectively.

The *MFF* mortality (%) was computed from the fraction of survivors using Equation S14.

$$MFF\ \text{mortality} = \left(1 - \frac{N(t)}{N_0}\right) \times 100 \quad \text{(S14)}$$

For model calibration, the reference lethality is 1.5552 x 10^6 s and the D_{Tref} is 3.7 days (Myburgh, 1965; Tang et al., 2007).

6. Thermal damage model for chilling injury

The thermal damage model for chilling injury is described in Equation S15. This model was calibrated using a methodology similar to the kinetic quality model.

$$\Omega(t) = \int_0^t k_{0,ci} \cdot e^{\left(-\frac{E_{a,ci}}{R.T_{rind}(t)}\right)} \cdot dt \quad \text{(S15)}$$

where Ω(t) is the damage integral as a function of time (-), $k_{0,\text{ci}}$ is the pre-exponential factor (s^{-1}), $E_{\text{a,ci}}$ is the activation energy ($J \cdot mol^{-1}$), and T_{rind}(t) is the temperature at rind (K) as a function of time. The damage integral (Ω) was calibrated using existing cold storage data for oranges to predict the severity of chilling injury damage. The severity is expressed as the portion of surface area of the rind (SA_{CI}, %) showing chilling injury symptoms. The calibration was based on iso-effect lines for various combinations of time-temperature exposure. Here, we assumed that citrus fruit stored at 1 °C for 21 days would have a damage integral of 0.0202, corresponding to about 2% of fruit developing chilling injury [62], [66], [67].

The damage integral (Ω) was further used to evaluate the probability of incidence of chilling injury ($CI_{\text{incidence}}$, %) using Equation S16.

$$CI_{incidence} = 100 \times [1 - e^{-\Omega}] \quad \text{(S16)}$$

We considered this probability index to be indicative of the percentage of fruits in the shipment showing symptoms of chilling injury.

7. Markov chain Monte Carlo method

Markov chain Monte Carlo (MCMC) is a class of algorithms used to generate a conditional posterior probability distribution of different sampled data to sample from it [68], [69]. The correlation coefficient between different parameters for the randomly generated population is often the same as the correlation coefficient of the sampled data.

Using MCMC, we generated a realistic 'virtual' population of 1000 oranges of different pre-harvest biological properties, including fruit size, fruit weight, TSS, fruit color, rind thickness and rind weight were considered for MCMC. Other pre-harvest biological properties, including fruit density, rind density, and fruit quality, were not considered for the MCMC as they were obtained from parameters used for the MCMC sampling. Additionally, other derived fruit properties such as thermal conductivity were not considered in this study because they did not provide extra information after our initial sensitivity analysis (result not shown in details) (e.g., for 1000 'virtual' population: mean thermal conductivity = 0.57, standard deviation = 0.004).

The implemented MCMC for this study has a total chain length of 3000, consisting of a burn-in period of 1000 iterations in order to reduce the number of unlikely occurrences in the posterior distribution. The learning and adaptation phases were performed from iteration 1000 to 3000 to evaluate the posterior distribution effectively. This procedure was performed for 2 independent runs.

The mean and standard deviation for the sample data and generated virtual population are shown in Table S1. By comparing the mean and standard deviation of sample data parameters and those of the virtual population, we see that these values are highly correlated, as expected.

Table S1. Mean and standard deviation of sample data and virtual population parameters.

		TSS (°Brix)	Fruit size [mm]	Average fruit weight [g]	Fruit color (scale 1-5)	Rind fresh weight [g]	Rind thickness [mm]
Sample data	Mean	10.25	77.06	251.26	2.04	3.87	6.51
	STDev	1.17	4.28	36.62	0.84	0.61	0.64
Virtual population	Mean	10.25	77.07	251.39	2.04	3.87	6.51
	STDev	1.26	4.79	39.87	0.94	0.69	0.73

8. Sample size determination

We used a modified Cochran's formula with 95% confidence level and ±5% precision to calculate the minimum required shipment size for the citrus supply chain (Equation S17) [20]:

$$n = \frac{n_0}{1+\frac{(n_0-1)}{N}} \quad \text{(S17)}$$

where n_0 is the random sample size (43), n is the modified sample size, and N is the population.

Figure S3 shows the relationship between air temperature and sample size. Particularly, the fluctuation of mean air temperature with the number of samples is shown in Figure S3a. It is evident that the temperature fluctuation is within the sensor accuracy range (1 °C) for a commercial citrus cold chain for a sample size of 5 and above. The very low-temperature deviation (<0.5 °C) for sample size above 5 further confirmed that the sample size used for postharvest variability assessment in this study was sufficient (Figure S3b).

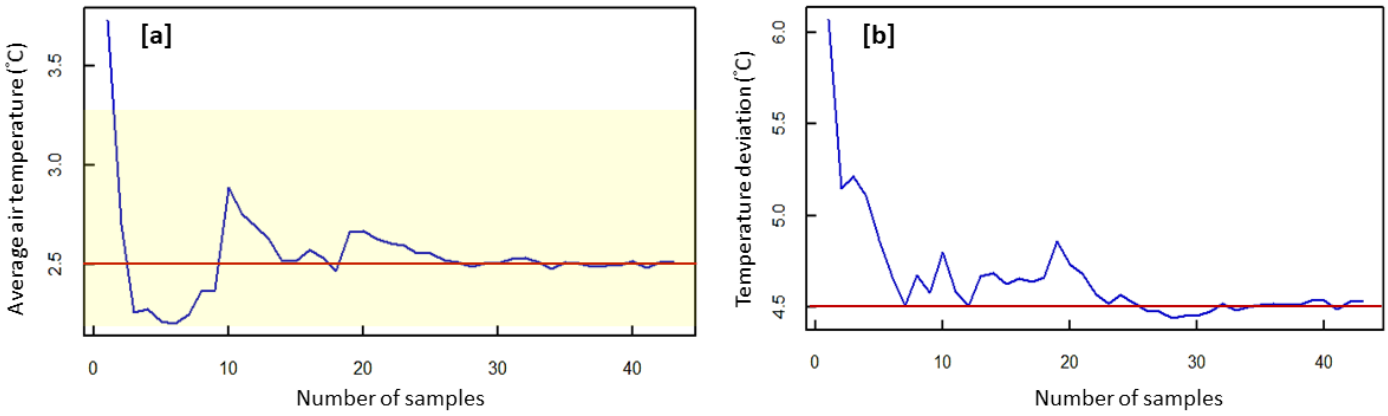

Figure S3. Sample size analysis showing: [a] the relationship between average air temperature and number of samples, and [b] the corresponding deviation of the mean temperature from the final mean temperature. The red-colored straight line represents the final mean temperature, while the yellow-shaded area represents the accuracy range of 1 °C for USDA approved temperature sensor.

9. Sensitivity analysis to quantify the impact of individual pre-harvest biological factors on fruit quality

We performed a sensitivity analysis to assess the contribution of each pre-harvest biological property of the fruit to the variability of the different quality evolution in the supply chain. By ranking each pre-harvest biological property, we can identify the management actions that should be improved to reduce postharvest losses in the citrus supply chain. Equation S18 [70] was used for this sensitivity analysis:

$$S = \frac{\partial x/x}{\partial p/p}\, x\, 100, \quad \text{(S18)}$$

where S is the percentage scaled relative sensitivity, ∂x is the change of values of fruit quality parameter, x is the fruit quality parameter, p represents the pre-and postharvest input parameters, and ∂p change of value of pre-and postharvest input parameters, at ±20% level in temporal scale.

The results of the sensitivity analysis are discussed here. The sensitivity analysis of mass loss is presented in Figure S4a. The most important pre-harvest biological factor contributing to up to 95% of the variability during shipping and at retail was a combination of fruit weight (70%), rind thickness (20%), and fruit size (5%). This suggests that controlling the fruit growth process (e.g., reducing cell number by controlling fruit temperature during the growing season) (Cowan et al., 2001; Okello et al., 2015; Quinet et al., 2019), and maintaining a good water management system and balanced nutritional program (NPK fertilizers) [74] could significantly reduce weight loss across the supply chain.

We observed that the fruit quality index variability during shipping and at retail is largely sensitive to initial fruit quality with more than 98% contribution (Figure S4b). A similar trend was observed for the remaining shelf life days, with initial quality contributing to more than 98% of the variability (Figure S4c). The fruit quality variability at harvest depends mostly on horticultural practices, including maintaining the health of the citrus fruit trees in the orchards. This is affected by several pre-harvest operations, such as irrigation, pruning, application of fertilizers, pesticides, and plant growth regulators [75]. Improving these cultural practices will reduce quality losses and increase shelf life at the end of the supply chain.

As already observed in section 3.2, the pre-harvest biological properties considered in this study contribute to less than 5% of the chilling injury variability during shipping and at retail (Figure S4d), with the amount of space occupied by fruits accounting for 3% during shipping and 2.5% at retail.

Note that the sensitivity analysis was not performed on MFF mortality, total soluble solids and color of oranges as the pre-harvest biological variability does not have a significant impact on these parameters across the citrus supply chain (see section 3.2).

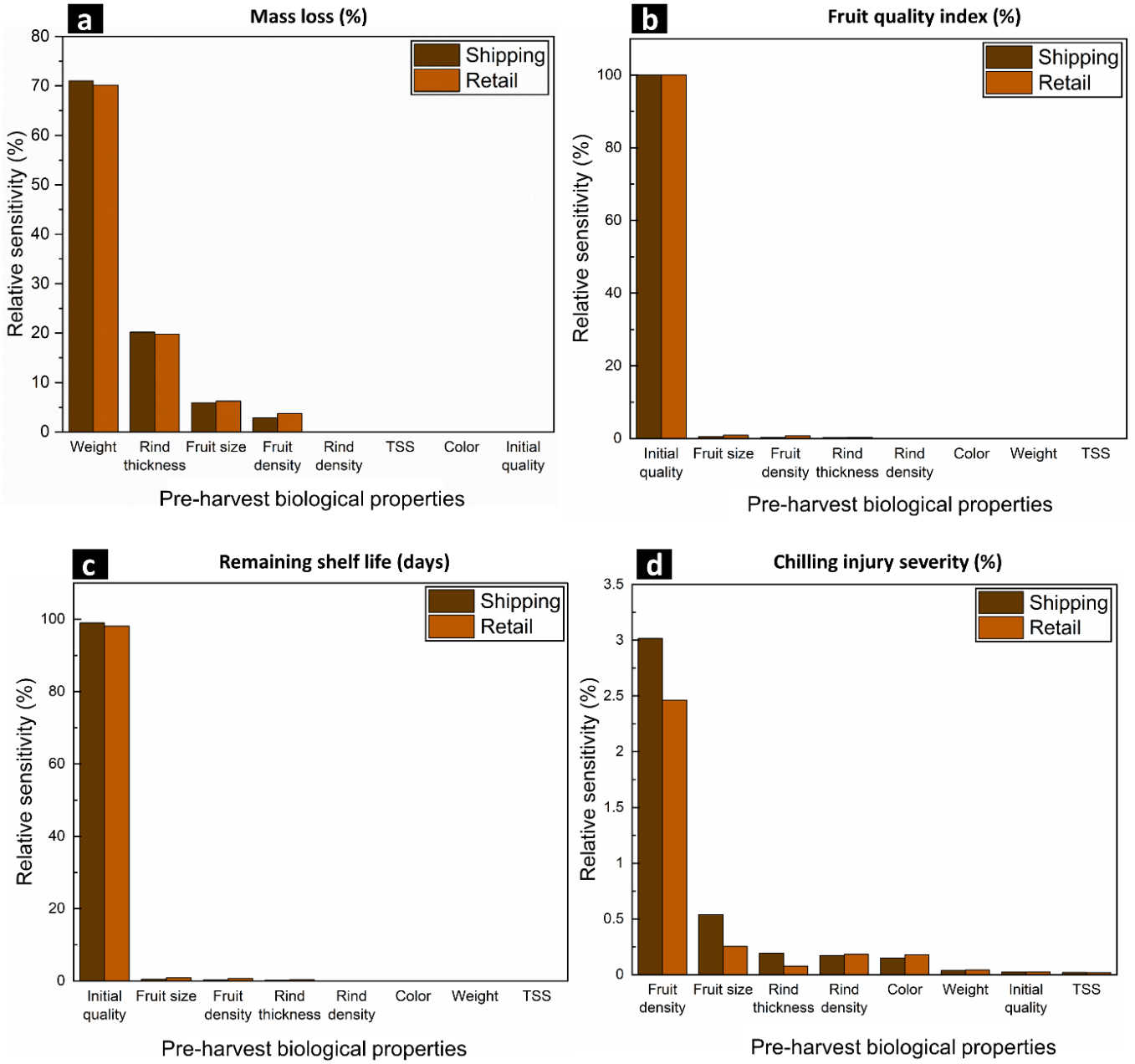

Figure S4. Impact of individual pre-harvest biological properties on (a) mass loss (%), (b) fruit quality index (%), (c) remaining shelf life (days), and (d) chilling injury (%) of oranges during shipping and at retail.

10. Grid sensitivity analysis

Based on a grid sensitivity analysis, an appropriate grid was constructed for the two-dimensional axisymmetric geometry of orange fruit. We evaluated four different grids: extreme-fine, base, extra-fine, and coarse grids with 11034, 6504, 2784 and 138 finite elements. The finest grid was the extreme-fine grid. A gradual refinement toward the air–rind and pulp interfaces was applied to enhance numerical accuracy and stability, as the largest gradients occur there. The differences with the extreme-fine grid are depicted in Figure S5 for the base, extra-fine and coarse grids for fruit surface and core temperatures. The plot shows that the difference with the extreme-fine grid for all selected grids is quite small. Therefore, the base grid was used in this study to optimize computational load and accuracy. This grid has a spatial discretization error on the local fruit surface and pulp temperatures below 0.002 °C. The grid consisted of triangular and quadrilateral finite elements, with a total element size of 6504.

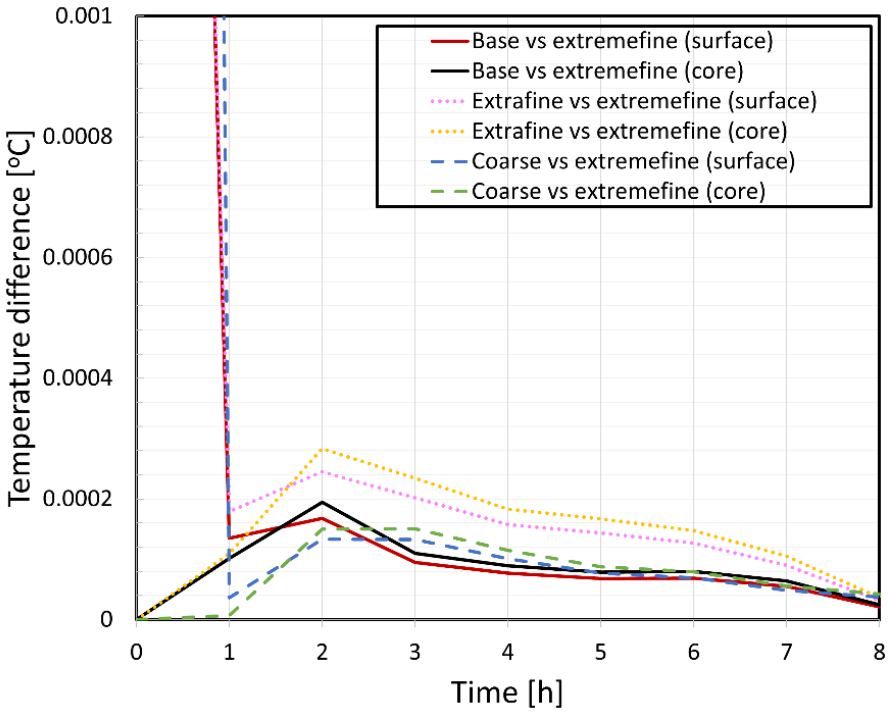

Figure S5. The difference in temperature of the base, extra fine, and coarse grid with the extreme fine grid as a function of time for the temperature at the surface and the fruit pulp core.